Cervantes-Montoya, Miguel Arturo

NONLINEAR OPTICAL INTERFEROMETERS

The University of Arizona PH.D. 1982

PLEASE NOTE:

In all cases this material has been filmed in the best possible way from the available copy. Problems encountered with this document have been identified here with a check mark __√__.

1. Glossy photographs or pages ____√____
2. Colored illustrations, paper or print _____
3. Photographs with dark background ____√____
4. Illustrations are poor copy _____
5. Pages with black marks, not original copy _____
6. Print shows through as there is text on both sides of page _____
7. Indistinct, broken or small print on several pages ____√____
8. Print exceeds margin requirements _____
9. Tightly bound copy with print lost in spine _____
10. Computer printout pages with indistinct print _____
11. Page(s) _____ lacking when material received, and not available from school or author.
12. Page(s) _____ seem to be missing in numbering only as text follows.
13. Two pages numbered _____. Text follows.
14. Curling and wrinkled pages _____
15. Other _____

NONLINEAR OPTICAL INTERFEROMETERS

by

Miguel Arturo Cervantes-Montoya

A Dissertation Submitted to the Faculty of the

COMMITTEE ON OPTICAL SCIENCES (GRADUATE)

In Partial Fulfillment of the Requirements
For the Degree of

DOCTOR OF PHILOSOPHY

In the Graduate College

THE UNIVERSITY OF ARIZONA

1 9 8 2

THE UNIVERSITY OF ARIZONA
GRADUATE COLLEGE

As members of the Final Examination Committee, we certify that we have read the dissertation prepared by Miguel Arturo Cervantes-Montoya entitled Nonlinear Optical Interferometers and recommend that it be accepted as fulfilling the dissertation requirement for the Degree of Doctor of Philosophy.

[signature]	6-18-82 Date
	Date
[signature]	1/4/82 Date
	Date
	Date

Final approval and acceptance of this dissertation is contingent upon the candidate's submission of the final copy of the dissertation to the Graduate College.

I hereby certify that I have read this dissertation prepared under my direction and recommend that it be accepted as fulfilling the dissertation requirement.

[signature] Dissertation Director	6-17-82 Date

STATEMENT BY AUTHOR

This dissertation has been submitted in partial fulfillment of requirements for an advanced degree at The University of Arizona and is deposited in the University Library to be made available to borrowers under rules of the Library.

Brief quotations from this dissertation are allowable without special permission, provided that accurate acknowledgment of source is made. Requests for permission for extended quotation from or reproduction of this manuscript in whole or in part may be granted by the head of the major department or the Dean of the Graduate College when in his judgment the proposed use of the material is in the interests of scholarship. In all other instances, however, permission must be obtained from the author.

SIGNED: 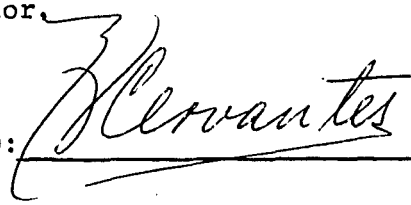

ACKNOWLEDGMENTS

I wish to express my deep gratitude to Professor Frederic A. Hopf, my dissertation director, whose advice and profound insight was so valuable in the elaboration of this work. He provided the guidance, patience, and encouragement necessary to complete such tasks. I hold his friendship very highly.

Many thanks to Professors Stephen F. Jacobs and George A. Stegeman for their participation as members of the dissertation committee, and for their suggestions, comments, and stimulating conversations. They kindly provided part of the equipment used in the experiments.

Thanks also to Dr. Akira Tomita for his participation in the preliminary experiments and who contributed a number of ideas to this work. To my fellow students, Ghanim Al-Jumaily, Till W. Liepmann, and Michael Soukup, my thanks for their fine friendship and help provided me during our laboratory work.

I also gratefully acknowledge the financial support provided by a Fellowship from Consejo Nacional de Ciencia y Tecnología of México.

For the preparation of this manuscript and general support, many thanks go to Norma Emptage.

Finally, a very special thanks to my wife, Ana Leticia, and our daughter, Berenice, in recognition of their support, patience, sacrifice and love.

TABLE OF CONTENTS

LIST OF ILLUSTRATIONS

LIST OF ILLUSTRATIONS--Continued

ABSTRACT

This dissertation is an experimental study of a novel type of interferometry based on the generation of Second Harmonic (SH) light. In this work interferometers are described in which an interference pattern arises when two SH waves are superimposed. These waves come from doubling the fundamental frequency of a laser by means of non-linear crystals.

Three interferometers are described that have different applications according to their sensitivity to detect wavefront distortions. One interferometer has low sensitivity and is useful in the contouring of refractive objects that produce large wavefront distortions of the order of hundreds of visible wavelengths. The other two interferometers have high sensitivity and one of them is capable of detecting wavefront distortions as small as 1/20 of wavelength.

Special emphasis is placed on development of the first interferometer which is a real-time, common-path, self-referencing interferometer that yields interferograms in the visible. The interferometer is based on the fact that a SH wavefront generated under PM conditions is a faithful replica of the laser wavefront. The two interfering SH wavefronts are produced one before and the other after the object under study, and by virtue of its chromatism, they are very slightly different. Consequently, very low density fringes are produced upon their superposition. In this application, noncritically phase matched crystals perform best, and we have found that Y-cut $LiNbO_3$ crystals configured for surface acousto-optic applications are very convenient. The

conversion efficiencies are very low (of the order of 10^{-5}) consequently optical damage to the $LiNbO_3$ due to the SH is no problem. The crystals are phase matched by controlling their temperature and are used with a repetitively pulsed Nd:Yag laser operating at 1.06 μm.

The chief limitations of this interferometer come from practical considerations in imaging objects with high spatial frequencies that reduce the contrast of the interferograms.

The high sensitivity interferometers make use of the changes of phase and amplitude induced in the SH wavefront by the phase mismatch of angle tuned crystals to provide information. The interferometers are directly sensitive to small wavefront tilts and do not require additional reference wavefronts.

CHAPTER 1

INTRODUCTION

This is an experimental study of interferometers based on the phenomenon of Second Harmonic Generation (SHG). SHG was the first nonlinear optical effect whose observation was made possible by the invention of high power lasers (Franken et al. 1961), and it is still one of the most convenient methods for producing higher frequency coherent radiation. SHG or frequency doubling occurs as a consequence of the nonlinearities of the polarization of certain classes of crystals in which in addition to the linear response, a field produces a component of the polarization proportional to the square of the field. The nonlinear response gives rise to the exchange of energy between an optical wave of frequency ν to a wave of frequency 2ν.

Interference, on the other hand, occurs when electromagnetic radiation follows more than one path from its source to the detection point. It can be described as variations in intensity as a result of the vector sum of two or more waves. Dark and bright bands or "fringes" are observed that correspond to cancellation or reinforcement of the superimposing light waves.

Interferometry based on nonlinear processes or "nonlinear interferometry" is a term that can be used to describe the techniques derived from interferometers that use either nonlinear phase

conjugation (PC) (Yariv 1976, Hellwarth 1977) or Second Harmonic generation. PC interferometers were proposed by Hopf (1980) and the operation of two types of PC interferometers have been demonstrated (Bar-Joseph et al. 1981).

SH interferometers have been reported in principle and in operation (Hopf, Tomita and Al-Jumaily 1980; Hopf et al. 1981; Hopf and Cervantes 1981) and they are the object of study of this dissertation. In these interferometers interference occurs between SH waves whose frequency arises from doubling the fundamental frequency of a laser. This contrasts with conventional interferometers founded on linear processes where the frequency of the interfering waves remains unchanged.

To our knowledge, the only previous work involving interference of SH waves was done to determine the phase of the nonlinear susceptibility (Chang, Ducuing and Bloembergen 1965; Wynne and Bloembergen 1969; Miller and Nordland 1970 and 1972). In this technique the interference between the SH light produced by two crystals in series was observed to measure the nonlinear constants of crystal samples in an absolute way or with respect to reference samples.

The chief difference between this technique and the interferometers described in this work is that in the former the crystals themselves are tested, whereas in our technique either the crystals or a third object can be studied. Figure 1, which illustrates schematically the Nonlinear Fizeau interferometer described below, can be used to show the general concept of our interferometers. The object under study is placed between the nonlinear crystals each of which generate a SH wave.

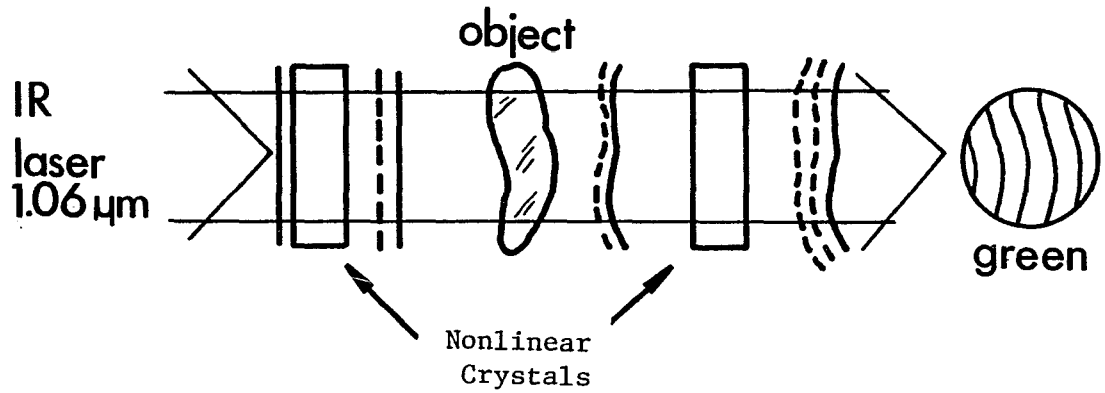

Figure 1. Schematic of a NLF interferometer.

The solid lines represent wavefronts at the laser wavelength λ_{IR} = 1.06 m; the dashed lines are SH (λ_S = .53 m) wavefronts.

At one point, both the fundamental and the SH tranverse the object and are distorted by the object. After the second frequency doubling occurs, we observe the interference between the two SH waves and from this we study the optical properties of the object that may vary spatially or temporaly or both.

In this work three interferometers are described that have found different applications according to the manner they respond to wavefront distortions. Much effort is devoted to the development of an interferometer that, because of similarities with Fizeau interferometers, we call nonlinear Fizeau (NLF). This interferometer is based on the use of phase matched crystals (Maker et al. 1962, Giordmaine 1962) and it relies on the dispersion of the object under study to produce interferograms of low fringe density. This allows us to study refractive objects that produce very large wavefront deformations and still the fringe densities and fringe distortions are kept reasonably low. The device is self-referencing, common-path and has real-time capability.

The major feature of the interferometer is the use of 90° phase matched crystals of $LiNbO_3$ configured for surface acousto-optical usages rather than for high efficiency SHG applications.

Interferometric methods of low sensitivity are useful when the objects being tested have large deformations which, when observed in conventional interferometers, produce fringes with very large spatial frequency that make the analysis of interferograms difficult. Three known alternatives to this interferometer that provide comparable interferometric information are: double immersion holography

Tsuruta et al. 1967); mid and far IR interferometry (Munnerlyn and Latta 1968) and two wavelength holography (TWH) (Wyant 1978). The first two alternatives can utilize cheaper lasers than the nonlinear approach and TWH. The infrared techniques involve some experimental difficulties due to detection and refractive elements perform differently at the wavelengths. The double immersion technique requires two separate steps and hence it cannot be implemented in real-time.

TWH has the advantage in the flexibility in changing the equivalent wavelength but attempts to make real-time common path TWH interferometry have proved disappointing due to Bragg angle problems (Lam, Koliopoulos and Wyant 1980). Hence, using TWH either involves abandoning real-time-usage or substantial alignment difficulties. For real-time applications with easy alignment at visible wavelengths, there are currently no alternatives to this nonlinear interferometer.

Note we have not included a detailed discussion of Moiré techniques since these are of use only for still larger deformations ($\gg$ 100 μm) than we are considering here.

The other two interferometers make use of distortions of phase and amplitude produced by phase mismatch of angle-matched crystals to provide information. These interferometers are sensitive to the slope of the wavefront rather than to the aberration of the wavefront and do not require an additional reference wavefront. One of these interferometers bears a superficial resemblance to a shearing interferometer; however, they differ in that as there is no deliberate shear introduced in the optical paths and the shear is generated by the wavefront slope

which is the rationale for calling this the Nonlinear Induced Shear interferometer (NLIS). The Maker fringe interferometer is based on the vanishing of the amplitude of the SH due to the phase mismatch between the fundamental and SH introduced by an angular deviation of the wavefront normals from the exact angle of phase match (Maker et al 1962).

Before proceeding to a description of the nonlinear interferometers, a suscint discussion of the relevant nonlinear optical concepts is presented. This is expected to serve as background for understanding the content of the remaining chapters. No attempt is made to give a comprehensive review of all the detailed work in this field, but emphasis is placed on the discussion of the physical processes underlying SHG.

Preliminary Concepts

Second harmonic generation comes from the interaction of an oscillating electric field with electrons in a crystal. When a light wave passes through a transparent crystal, an oscillating electric field drives the positive charge of the nucleus in one direction and the negatively charge cloud of electrons in the opposite direction. The nucleus being much heavier than the electrons is not capable of responding to the rapidly changing electric field, whereas the electrons of the outer shell respond rapidly to the oscillating field. The electrons of the inner shells stay tightly bound to the nucleus and are not affected in a significant way. The displacement of charges in opposite directions induces dipole moments on the atoms whose magnitude varies

according to the amplitude of the oscillating field. This induces a polarization in the crystal which is in phase with the driving field.

The crystal behaves as a highly directional antenna carrying an alternating current wave that travels through the crystal precisely in phase with the parent wave and radiating an electromagnetic wave travelling mainly in the same direction as the field which induces the polarization.

The energy of the driving wave remains essentially unaltered and the effect of the polarization wave and its subsequent reemission of light is to reduce the apparent velocity of the light wave through the crystal.

The situation is radically different when the intensity of the driving field is very high.

The light produced by some lasers when focused possesses an electric field of the order of 10^7 volts/cm that is comparable to the local interatomic fields inside the crystal, namely between 10^8 to 10^{10} volts/cm. Consequently when laser beams of such an intensity pass through a transparent crystal, a very large displacement of electrons is produced and, as a result the polarization is no longer proportional to the inducing field. Moreover, electric fields of the order of 10^7 volts/cm or more can cause damage to some materials. To illustrate what happens in this case, let us consider the motion of the valance electrons in an atom. Let r be the displacement of one of these electrons with respect to the equilibrium position and N be the volume density of electrons. The polarization P is given by

$$P(t) = - Ner(t) \tag{1}$$

The potential energy of an electron can be written as:

$$U(r) = \frac{1}{2} k_1 r^2 + \frac{1}{3} k_2 r^3 + \ldots \tag{2}$$

where k_1, k_2 are constants. This potential must reflect the symmetry of the crystal. In centro-symmetric crystals $U(r) = (U-r)$ so that the odd power terms in the potential vanish. These are of no interest here, since this condition rules out SHG, so that we concentrate on nonsymmetrical crystals where the condition $U(r) = U(-r)$ is no longer valid. This gives a restoring force

$$F = -k_1 r - k_2 r^2 \ . \tag{3}$$

The first term gives rise to thelinear polarization and the second gives the nonlinear polarization. Note that a positive displacement (r 0) results in a stronger restoring force (assuming that k_2 0) than that produced by a negative displacement. It immediately follows that if the field acting on the electrons is negative, the induced polarization is smaller than that induced when the field points in the opposite direction. This situation is depicted in Fig. 2 p. 16 which shows diagramatically the characteristic response of nonlinear materials in the presence of a moderately intense and a very intense electric field. Note that a very intense field in the right direction induces a larger polarization than that induced by a field pointing in the opposite direction. Such behavior is observed only in crystals possessing

certain intrinsic assymetry in their structure or, to be more precise, when they lack a center of symmetry.

The distorted polarization wave travels with the same velocity as the parent wave and it can be shown that this distorted wave results in the superposition of three components: one whose frequency is equal to that of the driving field ω ; another one of frequency 2ω called the second harmonic; and a D.C. component of the polarization which is constant (frequency = 0).

The general relationship between the polarization P as a function of the strength of the electric field E can be written:

$$P = \chi E \ (1 + a_1 E + a_2 E^2 + \ldots) \ \ldots \quad . \tag{4}$$

The term χ is the linear polarization of order unity, and the a's are the nonlinear coefficients which are normally very small so that only laser light has sufficient intensity to produce detectable amounts of SH light. The precise relationship between P and E is of tensor form but it is sufficient for the present work to deal with the scalar form of Eq. 4.

Supposing that the external field is of the form: $E = E_o \cos \omega t$ and substituting in Eq. 4 we get (keeping terms up to second order):

$$P = \frac{1}{2} \chi a_1 E_o^{\,2} + \chi E_o \cos \omega t + \frac{1}{2} \chi a_1 R_o^{\,2} \cos 2\omega t \quad . \tag{5}$$

This expression for the polarization contains a D.C. term, the first harmonic, and the second harmonic. It can be seen that the term $a_1 E^2$ gives rise to the D.C. and the second harmonic.

A suitable material for the production of optical harmonics must be relatively transparent to the fundamental and the desired harmonic frequencies. In addition to this there are some important crystal-symmetry considerations that affect the choice of the material. The SH component of the polarization travels in phase with the fundamental wave and radiates the light of frequency 2ω in the same direction it travels. However, in the vast majority of the relatively transparent materials, the high frequencies travel more slowly than the low frequencies--the magnitude of the difference being a few percent--and this means that the SH light is delayed with respect to the SH polarizatior.

Clearly the light radiated by the SH polarization at any point is out of phase with the light it radiated earlier and the two SH waves interfere destructively.

The distance required by the SH polarization and the SH light to be completely out of phase, i.e., to have a 180° phase difference, is called the coherence length and ordinarily is of the order of 10 μm's. If the thickness of the crystal is made equal to the coherence length, the SH disappears. As a result of the interference, it is usually worthless to use crystals longer than 10 μm when generating harmonics.

A number of techniques have been proposed to overcome this difficulty in practice. The most commonly used exploit double refraction (birefringence) exhibited by some crystals. In this crystal light travels with a velocity that depends on the plane of vibration of the electric vector (ordinary or extra-ordinary). The phase match technique consists in making the fundamental wave propagate as an ordinary (or extraordinary) ray such that its velocity is equal to that of the SH

that propagates as an extraordinary (or ordinary) ray. Thus by properly choosing the direction of propagation of the SH, which determines the direction of the electric field, it is possible, in certain cases, to compensate the delay produced by dispersion on the SH light by a greater velocity of the e-ray.

The technique is applicable to both uniaxial or biaxial crystals; however, in this work we will specialize our discussion to uniaxials, since this is the kind of crystal we used in our experiments.

The use of the phase match technique has produced an increase in the coherence length from a few tens of microns to more than one centimeter. The conversion efficiency, defined as the ratio of the SH power to that of the fundamental, is increased by a factor of 10^6.

Formalism of Wave Propagation in Nonlinear Media

The general problem of the interactions between light waves in nonlinear dielectrics was worked out by Armstrong et al. (1962).

In this section we make the usual derivation of an expression for the complex amplitude of the SH wave that serves as a basis for the interferometric concepts explained below.

The basic scalar equations describing nonlinear parametric interactions between three optical fields are:

$$\frac{dE_1}{dz} = -\frac{\sigma_1}{2}\sqrt{\frac{\mu_o}{\varepsilon_1}}E_1 - \frac{i\omega_1}{2}\delta\sqrt{\frac{\mu_o}{\varepsilon_1}}\,E_3E_2^{*}\,e^{-i(K_3-K_2-K_1)z}$$

$$\frac{dE_2}{dz} = -\frac{\sigma_2}{2}\sqrt{\frac{\mu_o}{\varepsilon_2}}\,E_2^{*} + \frac{i\omega_2}{2}\delta\sqrt{\frac{\mu_o}{\varepsilon_2}}\,E_1E_3^{*}\,e^{-i(K_1-K_3+K_2)z} \qquad (6)$$

$$\frac{dE_3}{dz} = -\frac{3}{2}\sqrt{\frac{\mu_o}{3}}\,E_3 - \frac{i\omega_3}{2}\,\delta\sqrt{\frac{\mu_o}{3}}\,E_1E_2\,e^{-i(K_1+K_2-K_3)z}$$

Where the E_i $(i = 1,2,3)$ represents plane waves propagating in the z-direction with angular frequencies ω_i and wave vectors k_i:

$$E_i(z,t) = E_i(z)\,\cos(\omega_i t - k_i z) \qquad (7)$$

The symbol * meaning complex conjugate. So that the instantaneous total field is given by:

$$E = \sum_i E_i(z,t) \qquad (8)$$

These equations are derived (Armstrong et al. 1962) from Maxwell's equations under the following assumptions:

(1) The induced polarization is parallel to the inducing field and has the form:

$$P = e\chi E + P_{NL} \qquad (9)$$

where $P_{NL} = \delta E^2$ is the nonlinear polarization term and δ is the effective nonlinear coefficient that couples the fields between each other.

(2) The amplitudes $E_i(z)$ are slowly varying over a one wavelength period so that we can assume that

$$\left| K_i \frac{dE_i(2)}{dz} \right| >> \left| \frac{d^2E_i(z)}{dz^2} \right| \tag{10}$$

(3) An energy conservation relationship is satisfied by the interacting fields so that $\omega_1+\omega_2 = \omega_3$. The field oscillating at ω_3 is originated by the fields at ω_1 and ω_2. Physically, this means that a power flux occurs from the fields at ω_1 and ω_2 to ω_3.

We now specialize Equation 6 to the case of SH in which two of the three fields have the same frequency--namely $\omega_1 = \omega_2 = \omega$. In this case the first two equations in 6 are complex conjugate of each other and we need to consider only one of them. Taking the fundamental field as E_1 and the SH as E_3 we have $\omega_3 = \omega_1 + \omega_2 = 2\omega$. Also, it is assumed that the crystal is nonabsorbing at any of the frequencies involved and therefore $\sigma_i = o$. According to these assumptions, the last of Equations 6 is rewritten as:

$$\frac{dE_s}{dz} = - i \frac{\mu_o}{\epsilon_s} \delta[E_F(z)]^2 e^{i\Delta Kz} \tag{11}$$

where $\Delta K = K_s - 2K_F$. Here "s" and "F" label the second harmonic and fundamental amplitudes respectively.

To simplify the analysis even more, it is assumed that the conversion efficiency is very small so that the depletion of the

fundamental due to the power transfer from ω to 2ω is negligible. Under these conditions that are valid in our experiments, we make $E_F(z)$ = constant in Equation 11 and also, supposing that the SH is nonexisting before the crystal, i.e., $E_s\ (z=0) = 0$, we obtain by integrating Eq. 11 over the length of the crystal ℓ.

$$E_s(\ell) = -i\omega \frac{\mu_o}{\varepsilon_s} \delta [E_F]^2 \frac{e^{i\Delta K\ell}-1}{i\Delta K}$$

using

$$\frac{1}{\varepsilon_s \mu_o} \triangleq \frac{c}{n_s} \text{ and } \lambda_F = 2\lambda_s \ .$$

This equation becomes:

$$E_s(\ell) = -i \frac{\pi c^2 \mu_o \ell}{n_s \lambda_s} (E_F)^2 \frac{\sin(\frac{\Delta K\ell}{2})}{\frac{\Delta K\ell}{2}} e^{i\Delta K\ell/2} \qquad (12)$$

This is the fundamental equation of this work. Note that if $\Delta K \neq 0$ both the intensity and the phase of the SH are affected whereas if $\Delta K = 0$ the intensity of the SH is proportional to the square of the intensity of the fundamental and the square of the length of the crystal ℓ.

ΔK can be written as a function of the refractive indices as follows:

$$\Delta K = K_s - 2K_F = \frac{2\pi}{\lambda_s}(n_s - n_F) \qquad (13)$$

where n_s, and n_F are the refractive indices of the crystal at the SH and fundamental vacuum wavelengths λ_s, λ_F. By making $n_s = n_F$, i.e.

by matching the indices, we have phase matching and both the second harmonic and fundamental beams travel with equal phase velocities inside the crystal.

If $\Delta K \neq 0$ the SH generated at some plane, say Z_1 having propagated to some other plane Z_2 is out of phase with the SH generated at Z_2. This results in the interference described by the factor

$$\frac{\sin (\Delta K \ell/2)}{\Delta K \ell/2} \tag{14}$$

two consecutive maxima of this spatial interference pattern are separated by the coherence length defined by

$$\begin{aligned} \ell_c &= \frac{2\pi}{\Delta K} \\ &= \frac{\lambda_F}{2(n_s - n_c)} \end{aligned} \tag{15}$$

and we see that the index matching condition is equivalent to having an infinite coherence length.

In practice the index matching requirement is obtained by following various method. However, we will be exclusively concerned with the two most widely used methods that we discuss in more detail next.

Angle Phase Matching

This approach due to Maker et al. (1962) and Giordmaine (1962) uses the natural birrefringence of the doubling crystals.[1]

---

1. The terms doubling crystal and doubler will be used indistinctively in this work.

In normally dispersive materials the refractive index of the ordinary wave or the extraordinary wave along a given direction increases with the frequency ω, and thus it is impossible to satisfy the condition $n_F = n_s$ if both the SH and the fundamental beams have the same polarization. We can, however, under certain circumstances satisfy this condition by making the two waves be of different type of polarization. To illustrate this point, consider a uniaxial crystal like L_iIO_3 or KDP in which the extraordinary index depends on the angle between the optic axis and the propagation direction. This is shown in Figure 2 for a negative ($n_e < n_o$) crystal.

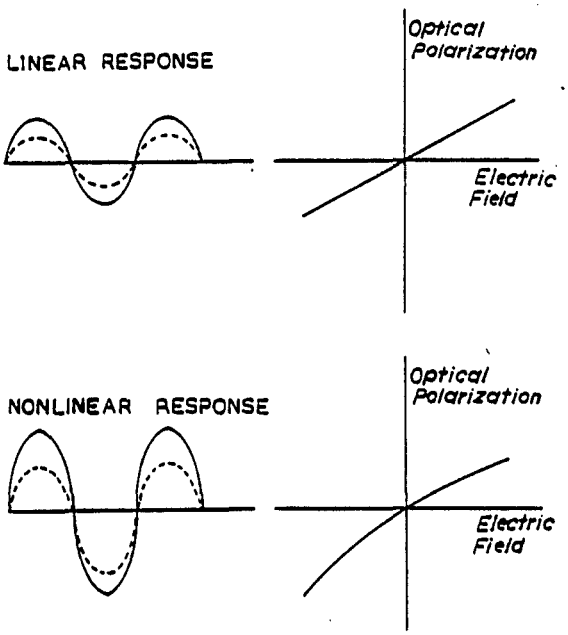

Figure 2. Illustrating the response to a driving field by linear and nonlinear materials.

If the fundamental beam is launched as an ordinary ray, the SH will be generated as an extraordinary ray and there will be an angle θ_{PM} at which

$$n_F^o = n_s^e \tag{16}$$

This direction is determinated by the intersection of the sphere that represents the ordinary index at ω (shown as a circle in Figure 2) and the surface that represents the extraordinary index at 2ω. That is given by (Rossi, 1962)

$$n_s^e(\theta) = n_s^o n_s^e \,/\sqrt{(n_s^o)^2 \sin^2\theta + (n_s^e)^2 \cos^2\theta} \tag{17}$$

The index matching would occur for all the wavelengths for which the ordinary index is larger than the extraordinary index at $\lambda/2$. The phase matching angle is calculated by substituting $n_s^e(\theta_{PM}) = n_F^o$ in Eq. 17 and solving for θ_{PM}

$$\sin\theta_{PM} = \frac{\frac{1}{(n_F^o)^2} - \frac{1}{(n_s^o)^2}}{2/(n_s^e)^2 - 1/(n_s^o)^2} \tag{18}$$

In this example we made the fundamental correspond to the ordinary and the SH to the extraordinary for the crystal is negative. For positive uniaxials the procedure is reversed, i.e., F→e and SH→o.

Returning to Equation 12, we see that when $\Delta K\ell/2 = m\pi$ the amplitude of the SH wave becomes zero and the SH vanishes. This

is called a Maker fringe after P. D. Maker et al. (1962) who demonstrated the dependence of SH intensity with the dispersion of the crystal.

The first Maker fringe occurs for m = 1 and this corresponds to an angular deviation $\Delta\theta$ from the exact phase match angle θ_{PM}. $\Delta\theta$ is a measure of how critical the setting of θ_{PM} is. $\Delta\theta$ is calculated by differentiating Eq. 17 with respect to θ, and using $\Delta K = \frac{2\pi}{\ell}$ we get

$$\Delta\theta = \frac{\lambda_F}{\ell} \frac{1}{\left[(n_F^o)^3 \left(\frac{1}{(n_s^e)^2} - \frac{1}{(n_s^o)^2}\right)\right] \sin 2\theta_{PM}} \tag{19}$$

this angle is found to be 0.022 degrees for a 1 cm. long L_iIO_3 for which $\theta_{PM} = 29.93°$.

Another feature of angle phase matching is the phenomenon of walk-off that occurs when the wave normals and the ray direction (direction of energy flow) do not coincide. It can be shown (Zernike and Midwinter, 1973) that these directions coincide only when $\theta = 0°, 90°$.

Therefore, in a phase matched interaction at an intermediate angle, the extraordinary beam does not overlap the ordinary beam in the entire interaction length.

Temperature Phase-Matching

Miller, Boyd and Savage (1965) showed that it is possible to have $\Delta k = 0$ and $\theta_{PM} = 90°$ by adjusting the temperature of the crystal. They found that the extraordinary index of some crystals is much more dependent on the temperature than the ordinary index, and by changing the temperature of the crystal to the right value, called the temperature of phase match, it is possible to alter the birrefringence until the ordinary and the extraordinary indices can be equal. In this case both the fundamental and the SH can be made to propagate perpendicularly to the optic axis. A necessary condition for 90° phase matching to occur is that

$$\frac{d}{dT}\left(n_s^e - n_F^o\right) \neq 0 \tag{20}$$

i.e., the rates of change of each index with temperature should be different.

An immediate consequence of this approach is that walk-off is nonexistent because $\theta_{PM} = 90°$ and to first approximation both beams propagate collinearly.

Another feature is that for $= 90°$, Eq. 19 becomes:

$$\Delta\theta = \frac{\lambda_F}{\ell}\left[\frac{1}{(n_F^o)^3}\frac{1}{\left[\frac{1}{(n_s^e)^2} - \frac{1}{(n_s^o)^2}\right]} - \right]^{1/2} \tag{21}$$

because then $\sin 2\theta_{PM} \cdot \Delta\theta \simeq 2(\Delta\theta)^2$ for $\theta_{PM} = 90°$ and the allowable divergence of the fundamental beam is larger than that of angle matching and is proportional to $\ell^{-1/2}$ rather than ℓ^{-1} as is the case in angle matching.

For these reasons 90° (or temperature) phase matching is also referred to as noncritical phase matching (NCPM).

In Figure 2 this corresponds to a situation in which the surface labeled n_s^e touches that of n_F^o at all points where $\theta = 90°$.

CHAPTER 2

THREE SECOND HARMONIC INTERFEROMETERS

In this chapter we describe the experimental equipment used in our laboratory and we describe one interferometer based on phase-matched SHG and two interferometers based on phase-mismatched SHG are discussed in principle and in operation.

Description of the Experimental Equipment

The Laser

The laser used in the experiments described throughout this work is a Nd:Yag (Geusic, Marcos, and VanUitert 1964; Kushida, Marcos and Geusic 1968) operating at room temperature whose lasing wavelength is 1.06 μm. When electro-optically Q-switched by a KD*P crystal it produced pulses whose peak power was between 50 and 100 KW and the duration of the pulses was approximately 20 nanoseconds. The pulse repetition rate could be changed from 0.5 to 10 Hz. The laser was optically pumped with a xenon lamp. The unexpanded laser beam was about 1 mm in diameter and it was linearly polarized in the horizontal direction.

The Crystals

Several kinds of nonlinear crystals were used to double the laser frequency to $\lambda = 0.53$ μm (green).

Lithium meta-niobate ($LiNbO_3$) (Boyd et al., 1964) was the most widely used crystal and it was used whenever a NCPM is mentioned in this work.

Lithium Iodate ($LiIO_3$) (Nath and Haussül 1969) was mostly used when a CPM crystal was called for.

Also, Potasium dihydrogen phosphate (KH_2PO_4) (Zernike, 1964) also known as KDP and lithium formate ($LiChO_2$-H_2O) (Singh et al. 1970) were occasionally used as angle tuned doublers.

Crystal sizes for the angle tuned $LiIO_3$, KDP and $LiChO_2 \cdot H_2O$ were 10 x 10 x 10 mm and the samples of $LiNbO_3$ ranged from 9 x 12 x 1 mm to 50 x 50 x 3.1 mm. The NCPM condition requires that the $LiNbO_3$ crystals be kept at the phase-match temperature and this was conveniently achieved with thermoelectric coolers of sizes 25 x 25 x 5 mm (Melcor, Trenton, NJ) that could maintain the temperature of pahse-match within ± 1°C. by adjusting the current supply. The phase-match temperature of the different $LiNbO_3$ samples ranged between 3°C to 15°C.

Recording of Observations

Ordinary black and white photographic film was mostly used in a 35 mm camera. Photographic speeds ranged from ASA 32 to ASA 400. Occasionally a TV camera was also used.

The Nonlinear Fizeau

In the previous chapter we obtained the equation that gives the complex amplitude of the SH as a function of the parameters

of the crystal and the amplitude of the fundamental. When phase-matching condition prevails, equation 7 becomes

$$\varepsilon^{2\omega}(\ell) = -i\frac{\pi c^2 \mu_o \ell}{n_s \lambda_s} [\varepsilon^{\omega}]^2 \qquad (22)$$

We note in this equation that the phase of the SH is twice that of the fundamental but because the SH wavelength is exactly one half the fundamental wavelength, this means that the phase front of the SH is a faithful replica of the fundamental phase front. This wavefront replicating feature of SH under phase matched conditions is the basis for the interferometer described in this section. This configuration, called the nonlinear Fizeau (NLF) interferometer relies on dispersion to produce a phase difference between the SH waves that generate an interference pattern. The principle of the NLF is illustrated in Figure 3 for the case of plane wave illumination.

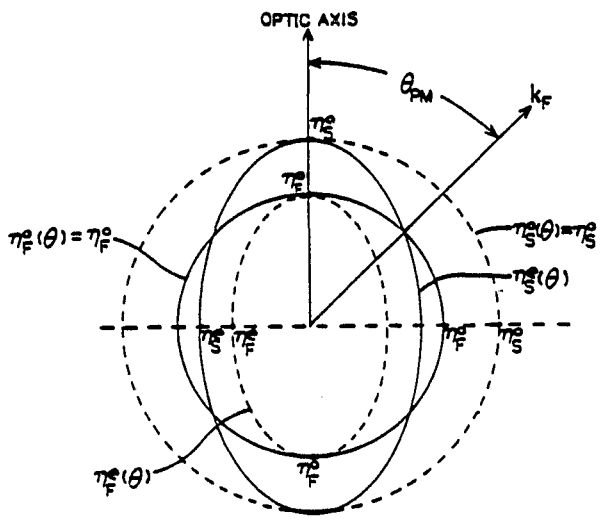

Figure 3. Index surfaces for the ordinary and extraordinary waves in a negative uniaxial crystal.

The phase-match condition is satisfied for the directions k_F in which $n_s^e(\theta) = n_F^o$. The excentricities shown are greatly exaggerated.

Two NCPM doublers are placed one before and another after the object being tested. The first doubler faithfully replicates the laser wavefront to produce two identical wavefronts that probe the object. The object itself has to be relatively transparent to both the laser and SH frequencies. After traversing the object, both wavefronts are distorted according to the physical thickness and the refractive index each frequency "sees" in the refractive object. Then the second crystal replicates the structure of the distorted laser wavefront producing another SH beam that interferes with the SH produced by the first doubler. The laser beam is then disposed for safety reasons and one observes the fringes in the SH or, in this case, in the green. Since the interfering wavefronts differ only by the chromatism of the object the fringes are much more widely spaced than the fringes we could get by interfering either wavefront against a plane reference wavefront.

The chief difference between this configuration and the non-linear Twyman-Green interferometer described elsewhere (Hopf et al., 1980) is that here both the IR and green beams pass through the object and emerge with different wavefronts due to its dispersion. When the laser is doubled for the second time, the difference in phase between the two green beams is

$$\frac{2\pi}{\lambda_s}\,\ell(n_S-n_F) \tag{23}$$

giving bright fringes when this is equal to $2m\pi$. Solving for ℓ gives:

$$\ell(x,y) = m\frac{\lambda_s}{(n_S-n_F)} \tag{24}$$

where $\ell(x,y)$ is the physical thickness of the object, n_S and n_F are the vacuum refractive indices at the second harmonic and fundamental, and m is an integer.

By comparison with conventional interference patterns, the fringes are coarser by a factor $1/(n_S-n_F) \sim 100$. So, one can study objects that are optically very deep (hundreds of visible wavelengths) and still get a conveniently low fringe density.

The object can also be a surface immersed in a dispersive liquid and then the NLF becomes analogous to the immersion method in holography (Tsuruta et al. 1967) in which the medium surrounding the object is changed between two photographic exposures giving a fringe pattern with an equivalent wavelength $\lambda/\Delta n$.

In the case of the NLF $\Delta n = n_S-n_F$ and this means that one can get different fringe densities by choosing different dispersive liquids.

The simplest test of the NLF uses a glass (BK-7) wedge whose dispersion was calculated using a Sellmeier formula (Schott glass data book, page II-5). The wedge was placed in the interferometer introducing an angular separation between the probe wavefronts that produced straight fringes whose spacing coincided with that predicted by using the calculated dispersion and the measured angle of the wedge.

The Maker Fringe Interferometer

In this section and the following one we discuss interferometers in which the phase mismatch of an angle tuned doubler is the key to forming the interference patterns.

In Chapter 1 we saw that when the factor ΔK in Equation 12 does not vanish, then both the amplitude and phase of the SH wave are affected by the magnitude of this mistatch. Rewriting Equation 12

$$E_S = \beta \frac{\sin \frac{\Delta K \ell}{2}}{\frac{\Delta K \ell}{2}} \exp\left(\frac{i\Delta K}{2}\right)$$

where

$$\beta \equiv - \frac{i \pi c^2 \mu_o \ell}{n_S \lambda_s} \delta [E_F]^2 \qquad (12)$$

When the fundamental is polarized as an o-ray and the SH as an e-ray, the mismatch $\Delta K = K^{2\omega} - 2K^{\omega}$ is given by Equation 15. In the case of CPM one of the indices, usually n_S, depends on the angle of tilt θ between the phasefront normal and the optic axis. This dependence is utilized to set $\Delta K = 0$ at $\theta - \theta_{pm}$ when desired. Tilts of the wavefront cause ΔK to depart from zero and thus a mismatch is introduced. This results in the amplitude and phase perturbations in the green wavefront described by the two terms in brackets in Equation 14, which are the basis for the two interferometers described below. The first is based on the effect of the mismatch introduced by the wavefront aberration on the amplitude (first bracket) and is referred to as Maker fringe (MF) interferometer. The other, called the nonlinear induced shear (NLIS) interferometer depends upon the effect of the mismatch on the phase term (second bracket).

The principle of the MF is based on the fact that the sine term in Equation 7 vanishes whenever $\Delta K \ell/2 = m$ (m can be all integers but zero) giving dark fringes in the intensity of the SH. Suppose

we take the example of an interaction where n_S is angle dependent and n_F is angle-independent. Let us take the coordinate z to describe the direction of propagation of the light and let the optic axis lie in the y-z plane. We then call y and z the critical and noncritical dimension respectively. The Maker Fringe appears in the y direction whenever

$$\frac{2\pi}{\lambda_S}\,[n_S(\theta) - n_F]\frac{\ell}{2} = m\pi$$

or, using Equation 19

$$\frac{1}{2}\,\frac{\ell}{\lambda_s}\,\frac{n_F^3\,(n_o^2 - n_e^2)\,\sin 2\theta_{PM}}{n_o^2\,n_e^2}\,(\theta - \theta_{PM}) = m \qquad (25)$$

here n_F is the ordinary index at λ_F, n_o and n_e are the ordinary and extraordinary indices at λ_S.

In the experiments, the primary analyzing crystal is always a CPM $LiIO_3$. When a second crystal was used, it was either a CPM $LiChO_2 \cdot H_2O$[2] or KDP.

The set up of Figure 4 is used for both the MF and NLIS interferometers.

---

2. Unlike the rest of the crystals used in our experiments, $LiChO_2 \cdot H_2O$ is biaxial. When used, it is oriented so that the plane polarized fundamental has one o-ray component and an e-ray component. This is called Type II phase matching. Type I occurs when the fundamental is either o-ray or e-ray.

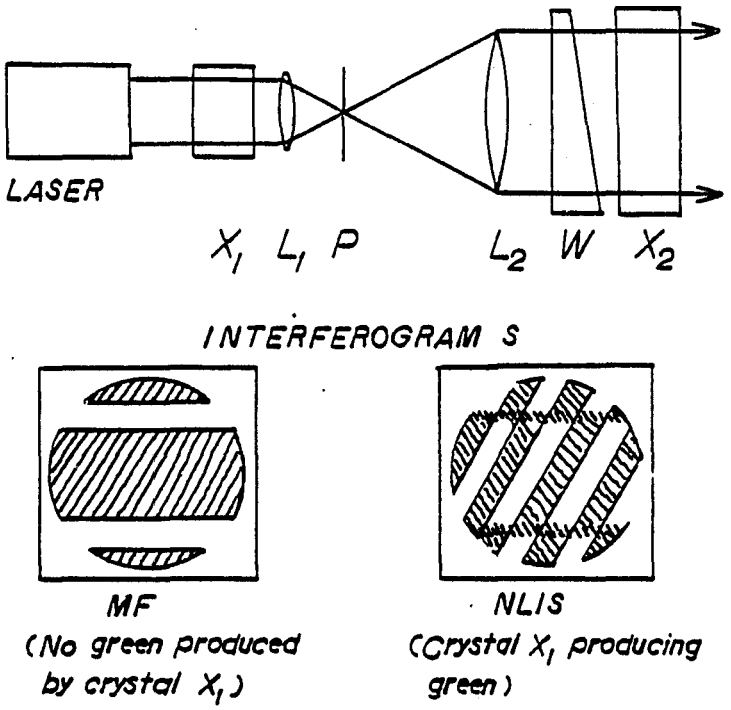

Figure 4. Schematic of a set up for MF and NLIS interferometers.

$X_{1,2}$: angle matched crystals, L_1,2: lenses, P: pinhole, W: 2° wedged glass blank. In the MF interferometer (see Figs. 5 a-c) the crystal X_1 is mistuned to generate no second harmonic. In the NLIS the crystal is tuned to generate second harmonic. In Fig. 5, the data is taken with X_1 between L_2 and the wedge W, and the object is between L_2 and X_1.

A collimating beam expander using lenses of 23 and 260 mm focal lengths was set up, in which the second lens was an achromat. The KDP doubler was placed before the first lens which, when phase matched, produced ample green light, and an aluminum foil was placed at the focal plane of the first lens, where a pinhole was burned. This pinhole eliminated the chromatism of the first lens by becoming a point source for both beams and resulted in the collimator being achromatic.

A 2° glass wedge whose use is explained below, and the $LiIO_3$ crystal was placed after the collimator.

When the KDP crystal is tuned far from phase matching, no green light emerged from the collimator and the green light generated by the $LiIO_3$ produced the pictures of figures 5 a-c, where the collimator gave slightly converging (Fig. 5a), collimated (Fig. 5b), and slightly diverging (Fig. 5c) light. The Maker Fringes appear in Figure 5a and 5c as horizontal black bands. Bright fringes above and below the central spot are visible to the eye but the film does not have the dynamic range to record them. Right after each picture was taken the KDP was phase matched to produce SH light. This gave rise to the interference fringes in Figures 5d - 5f. The vertical fringes are due to a tilt between the IR and green produced by the chromatism of the wedge, and the slight curvature of the fringes is an artifact of the residual chromatism of the achromat (this will be ignored in subsequent discussion). When the beam is a planewave, the fringes

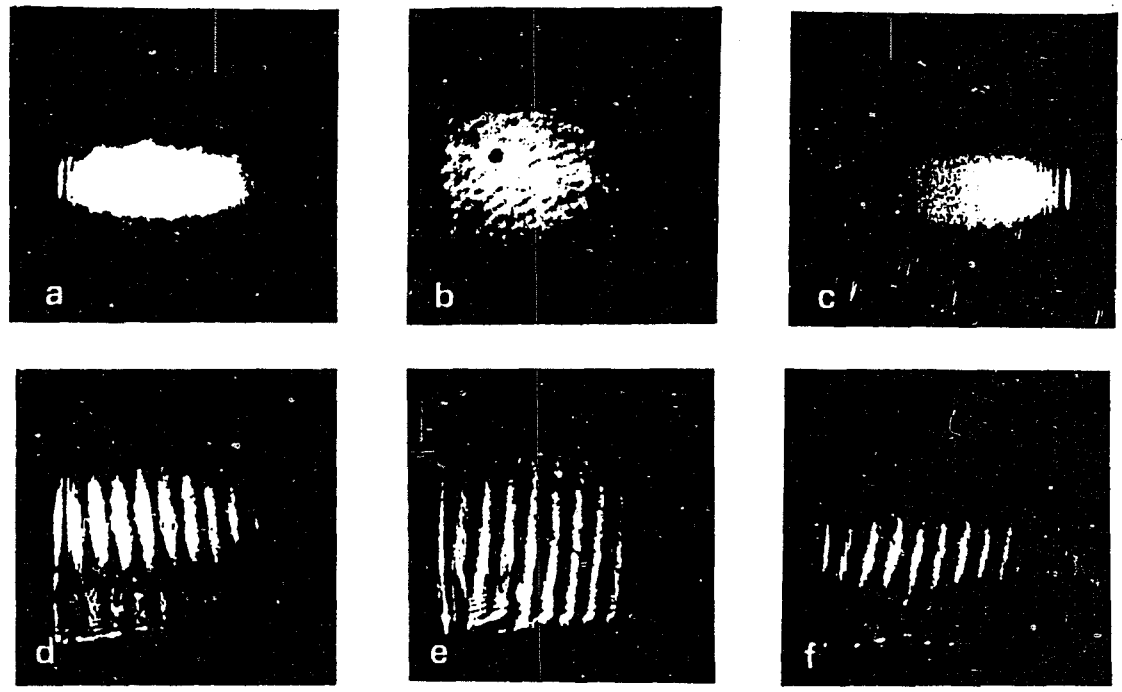

Figure 5. Maker Fringe interferograms.
See text for identification of a-f above.

vertical as seen in Fig. 5e. When the wavefronts are curved, the fringes are tilted as shown in Fig. 5d and 5f. This tilt comes from the displacement of the disturbance due to the linear dependence of ΔK on θ in Equation 12. The displacement effect is similar to those of a shearing interferometer. When the "sinc" function in Equation 12 changes sign, the bright and dark fringes interchanges which gives an apparent motion of $\lambda/2$ to the fringes at the location of the Maker Fringe. This is seen in Fig. 5d and 5f.

The Nonlinear Induced Shear Interferometer

We now consider the effect of the term in the second bracket i.e., the phase term, and let us suppose first that $\Delta K\ell/2 < m\pi$ everywhere across the beam. In other words, there are no Maker Fringes. In this case the phase term causes a phase aberration in the green whose local magnitude is equal to π times the left side of Equation 25.

The NLIS interferometer can be constructed using two doubling crystals. If the first crystal is NCPM, it generates a wavefront in the green that is a faithful replica of the wavefront of the fundamental, which is used as a reference wavefront. The second crystal which is CPM has an additional phase distortion due to the term $\Delta K\ell/2$ in the exponent of Equation 12. By observing the interference pattern between these two SH's, one can measure the amount of the induced phase distortion, which is related to the local wavefront tilt according to Equation 4. The interferometer can be made sensitive to both x and y directions by using a CPM crystal, as first doubler

instead of the NCPM whose critical dimension is perpendicular to that of the second doubler. In this way the aberrations induced by the two crystals are orthogonal to each other.

A potential application of the NLIS is to enhance a phase distortion whose depth is small to be measured by conventional interferometers (e.g., a Twyman-Green). Since the induced phase distortion depends on the local wavefront tilt, which can be changed by the lateral magnification of the wavefront, the induced phase change can exceed the original phase distortion.

To show this we use the setup shown in Figure 4. First we remove the crystal X_1 (i.e., the KDP) and use instead a $LiChO_2$-H_2O crystal that we locate just in front of the wedge. The critical dimension of the $LiChO_2$ is orthogonal to that of the $LiIO_3$, and we use a one dimensional phase object oriented so that the $LiChO_2$ acts as if it were noncritically phase matched, i.e., it generates a wavefront at the SH that is a faithful replica of the fundamental (a NCPM crystal would be ideal for this purpose but when this experiment was performed such a crystal was not available to us).

The phase-object is a groove of 0.14 mm width polished in a microscope slide. It is partially index matched to have a 1/10 λ_S septh as shown in a Jamin Interferogram in Fig. 5a. In order to increase the slope we demagnify the object by a factor of two with a collimating lens pair. The resulting NLIS interference pattern is shown in Fig. 6b. One sees that there is a $\lambda_S/5$ fringe motion, which is twice that of the fringe motion in Fig. 4a.

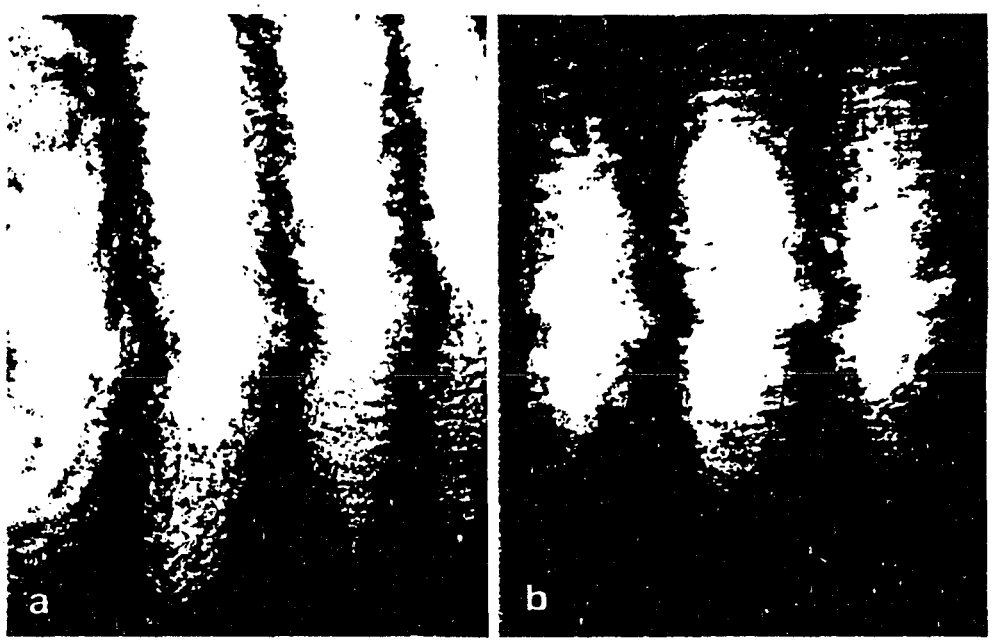

Figure 6. Interferogram of groove in Taimin and NLIS interferometers.

a. Interferogram of index-matched groove taken by Tamin interferometer.

b. NLIS interferogram of same subject.

Hence we have demonstrated that the NLIS is capable of enhancing the fringe motion, which cannot be done with conventional shearing interferometers.

We have performed a number of tests to compare the sensitivity of the SHI's with a wedged shearing interferometer. While the overall comparison is complicated, as a rule, the shearing interferometer reaches marginal sensitivity for phase front curvatures that are easily measured by the MF and NLIS. The NLIS is more sensitive than the MF and is much more sensitive than the shearing interferometer. Note, however, that the sensitivity of NLIS depends on the difference between n_o and n_e. Crystals with large $(n_o - n_e)$ such as $LiIO_3$ are more sensitive to tilts than those with small $(n_o - n_e)$ such as KDP.

CHAPTER 3

PRACTICAL VERSION OF A SECOND HARMONIC INTERFEROMETER

In Chapter 2 we discussed the concept of an interferometer that because of its similarity to the Fizeau interferometer, we called it nonlinear Fizeau (NLF) and demonstrated that it works. In this chapter we describe a breadboard version of the NLF that can serve as a useful instrument. We demonstrate that the NLF can usefully contour complex objects with large variations in optical depth that can also vary rapidly in time. We will see that its chief limitations come from practical considerations in imaging objects with high spatial frequency content, rather than in the nonlinear optics.

The Crystals

Since the interferometer provides information about the chromatic differences of the object, the initial common wavefront of the fundamental and SH is arbitrary and can be chosen for convenience (spherical is often useful). In concept, this also means that the NLF is independent of the quality of the laser beam, i.e., multimode lasers might be used. The problem here is that amplitude structure in the laser beam can be a very confusing feature in reading the fringes (it does not however, affect contrast), so we prefer to use a laser with a single TEM_{oo} transverse mode. Note also that a NCPM crystal is achromatic, so that it does not produce any difference

between the wavefront and hence the interferometer is not, in principle, affected by the figure of the doubler. If the figure is bad, one does have to use a setup in which one images the surface of the doubler onto the recording plane to avoid distorting the information. It is best then for the surfaces of the crystal to be flat, but there is no need for them to be parallel. The maintenance of a uniform phase-matching condition over the entire crystal is an essential requirement, since otherwise the doublers will not faithfully reproduce the wavefronts. For that reason, it is important that the crystal be homogeneous and that the temperature of phase-match be constant across it.

Lithium Niobate is a negative uniaxial as are many of the crystals that are commonly used in frequency doubling. Our discussion will be particularized for this case in which the fundamental is an o-ray and the SH is an e-ray. Note that frequency doubling automatically selects the proper polarization components from the laser beam so that one does not need to polarize the laser. Nevertheless it must have an o-ray component. Moreover since the SH polarization is always an e-ray, one ensures that the interfering SH waves have the same polarization by properly orienting the crystals.

Since we will be dealing with wavefronts which tilt in various ways with respect to the crystal, it is important to understand how these tilts affect the phase matching process. It is easier, however, to discuss the case where the wavefront is a plane wave and we tilt the crystal with respect to the wavefront. The response of the doubling to these tilts is highly asymetrical. If we rotate the

NCPM crystal about the optic axis, the phase matching is independent of angle. We call this "noncritical dimension" of tilt. If we tilt the crystal about an axis perpendicular to the optic axis, the index of the e-ray varies with angle and the pahse-match changes. We call this the "critical dimension" of tilt, which is characterized by the critical angle θ_c, which is the angle of tilt at which the second harmonic vanishes due to phase mismatch. We will show, explicitly, that it is possible to operate the interferometer at angles greater than $\pm\theta_c$, but this involves complications in the data analysis. We thus take $2\theta_c$ as the nominal acceptance angle of the crystal. For our NCPM crystals, θ_c is measured to be 4.5° which is equivalent to setting the smallest f-number of our beams at f/6.4.

In critical phase matching, the e-ray is not polarized parallel to the optic axis, and the polarization direction of the e-ray replaces the optic axis in the definition of the critical and noncritical dimensions. As a rule, the acceptance angle of the CPM crystal in the noncritical dimension is of the same order (usually several degrees) as the acceptance angle of an NCPM crystal in the critical dimension, and these angles decrease as $L^{-1/2}$. The critical angle of a CPM crystal is much smaller, typically about 10^{-4} rad., and it varies as L^{-1}, as can be seen in Equations 21 and 23.

The desirability of a large acceptance angle is only one of several reasons why the NLF needs crystals with short lengths. A more important reason is that the doubling efficiency must be kept very low in order to avoid damage to the eye or to the detection system.

Moreover, $LiNbO_3$ is peculiar among nonlinear optical materials in that its optical properties can be altered by moderately high radiation levels at the SH of the 1.06 μm laser (Ashkin et al. 1966). The low efficiencies of the NLF avoid this problem. In addition, the short lengths mean that the temperature tolerances of the NCPM condition are not very severe.

Conventional nonlinear optical applications call for high efficiencies and the appropriate crystals have small clear aperatures and large lengths. These are unsuited for the NLF. In contrast, Y-cut $LiNbO_3$ in its normal configuration for surface acousto-optical applications (Lean, White and Wilkinson 1976; Kim and Tsai, 1976) is ideal for the NLF, in that these samples have large clear apertures ranging from 2 x 2 to 5 x 5 cm^2 and short lengths ($\sim$ 2-3 mm). Our laser has peak powers of 50 Kw, and when the beam is expanded to areas of $\sim$ 4 cm^2, the resulting efficiencies are quite suitable ($\sim 10^{-6}$) for the NLF. Furthermore, the short lengths are such that even with a focussed laser beam, the SH intensity does not damage the sample (of course, it is damaged by high laser intensity just as any other material).

Lithium niobate grown for acousto-optic applications comes in two grades, acoustic and optical. The latter is made with purer components and is grown with greater care. We have found that this grade has always been suitable for our purposes. However, because of its higher purity, optical grade $LiNbO_3$ tends always to have a phase match temperature in a relatively limited range from 0° to 4°C, and one must provide a dry nitrogen atmosphere to prevent condensation.

Acoustic grade niobate is less pure, and hence its phase match temperature is more variable, ranging from 4°C to greater than room temperature for the samples we have tested. The bulk of our data was taken with a sample of Union Carbide acoustic grade material whose homogeneity has proved to be quite satisfactory, and which has a phase match temperature of 15°C at which condensation is not a problem. The temperature tolerance of all our $LiNbO_3$ samples was 2°C, which is sufficiently large that the material can be cooled from the edges and can maintain a sufficiently uniform temperature such that no departure from uniform phase matching is observed. We have developed a simple temperature-controlled mount for the $LiNbO_3$ crystal which we show in Figure 7a. This is in contrast with a typical commercial NCPM mount for high efficiency doubling that we shown in Figure 7b in which a sealed cell (right) is mounted inside an oven (left). Typical sealed cells cause severe vignetting (Hopf, Tomita and Al-Gumaily, 1980). They also prevent physical and optical access to the crystal so that some of the most useful setups of the NLF become impossible.

Setup of the Interferometer

In this section we discuss the basic considerations involved in setting up the interferometer. This can be conveniently divided into two separate steps which we deal with individually. 1) The first step provides the identical laser and SH wavefronts, and deals also with the problem of varying the SH intensity so that one can obtain good contrast in the interference pattern. This also provides a visible

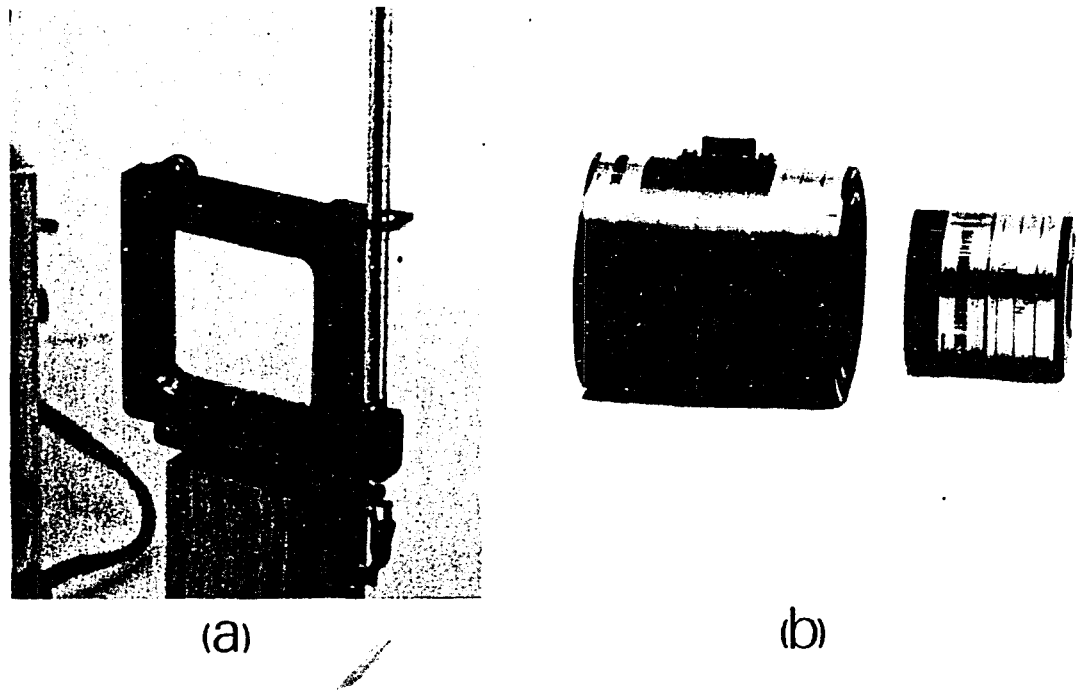

Figure 7. Mounts for temperature-tuned crystals.

(i.e., SH) beam that is useful for aligning the second half of the setup. 2) The second step involves illuminating the object, injecting reference fringes, making the second doubling step, and imaging the interference pattern.

Providing the Initial Wavefronts

Two alternative methods that we find very useful in carrying out the first step of the setup are illustrated in Figure 8. In Fig. 8a the doubling takes place first. Since the diameter of the laser beam is very small, the beams are expanded with a positive simple lens L that focuses both beams on a piece of aluminum foil where the laser burns a pinhole, p, a few tens of microns in diameter. The pinhole serves to eliminate the chromatism of lens L, and becomes a point source for both wavefronts. It also spatially filters the two beams.

In this configureation, X_1 is an angle tuned crystal (we use $LiIO_3$, but any Type I CPM doubler will work) and it has the advantage that small aperture crystals can be used. The intensity of the SH is changed in this case by tilting the crystal to an angle slightly different from the phase-matching angle. This allows optimization of the contrast of the NLF fringes. However, when the crystal is not phase-matched and the angle of incidence of the fundamental is not normal to the crystal surface, one finds (Bloembergen and Pershan 1962) that two SH beams are generated in the crystal, one of which follows a path that coincides with that of the fundamental, and the other follows a slightly different path inside the crystal. This phenomenon

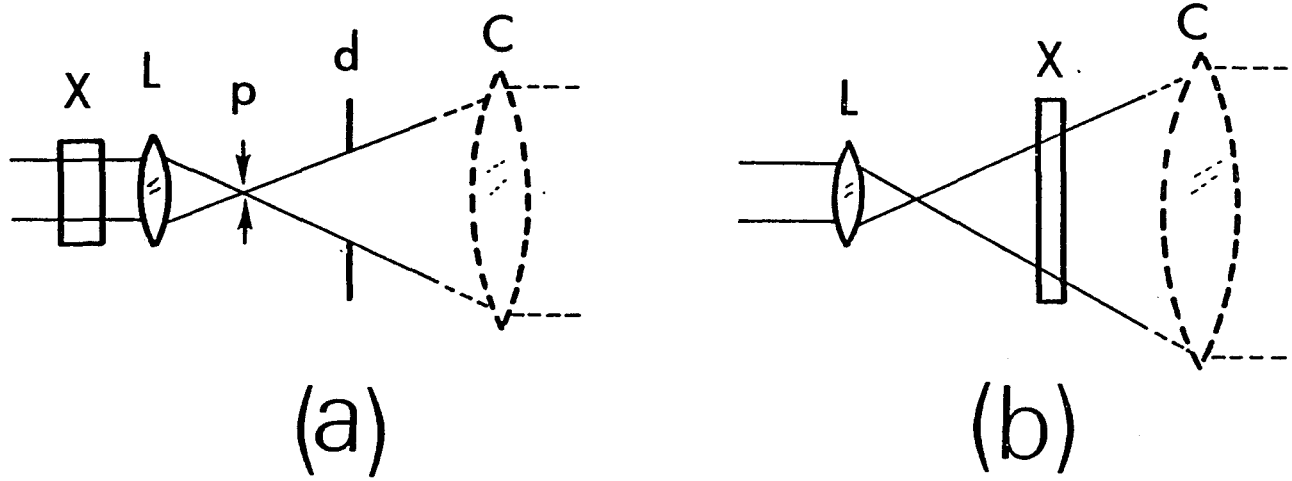

Figure 8. Schematic of two alternate setups for the first half of the NLF.

comes from the special character of the boundary-value problem of the SH waves. Both SH beams exit from the crystal and follow parallel trajectories from then on. The SH beam then appears as an elongated spot or as two spots which almost overlap. The NLF fringes appear only in the portion of the SH which overlaps the laser beam (this effect is shown explicitly in the NLF interferograms in Figure 8. If one uses the SH for subsequent alignment, the nonoverlapping part of the SH beam can be annoying and it is desirable to mask this part of the beam with an iris diaphragm, d.

In Figure 8b, the doubling occurs after the laser beam is expanded using either a positive or negative simple lens and it is made with an NCPM crystal of $LiNbO_3$ of large clear aperature. The intensity of the SH is controlled by placing the crystal at an appropriate location along the diverging fundamental beam. The SH power is quadratic in the laser power density, and the farther one is from the focal point, the less SH is produced. This can be used to adjust the contrast. If too much SH intensity is produced at the most expanded position, one can change the temperature of the crystal as a coarse adjustment of the SH power. In both configurations of Figure 8, the use of an achromatic lens or mirror, c, to collimate the beam is optinal (dotted drawing in Figure 8).

Contouring the Object

Figure 9 shows an idealized setup for the second half of the NLF. In order to make the NLF fringes more easily understood, it is

often desirable to start with straight reference fringes that are then distorted by the introduction of the object. This can be accomplished with a glass wedge W that produces an angular separation $\beta = \alpha_w \Delta n$ between the two probe wavefronts, where α_w is the wedge angle and Δn is the dispersion of the glass. The wedge is ideally positioned just before the object. Placing it after the object causes it to behave, in part, as a lateral shear interferometer and this could be misleading in the interpretation of the fringes. The wedge can also be placed directly in front of the doubler in the setup of Figure 9. The achromatic lens L_1 (or mirror) is used to image the object onto the second doubler X_2 and then lens L_2 relays the image onto the camera where the interferogram is recorded.

The greatest single source of difficulty in the interferometer is the imaging of the object onto the film. The objects of interest tend to have very high spatial frequency, and the imaging must be quite precise. This is the main objection to letting L_1 be a chromatic lens, since the two SH beams cannot be imaged onto the same plane.

The setup in Figure 9b in which L_1 is eliminated and L_2 images the object onto the film, is often a very effective and easy alternative to Figure 9a. This setup is equivalent, optically, to improperly locating the doubler in the setup in Figure 9a. We made extensive tests of the role of imaging onto the doubler in the setup of Figure 9a to evaluate the limitations of using the easier version. We have found that if there is an effect of imporper imaging (for some objects such as cylindrical and spherical lenses, there is no effect), it

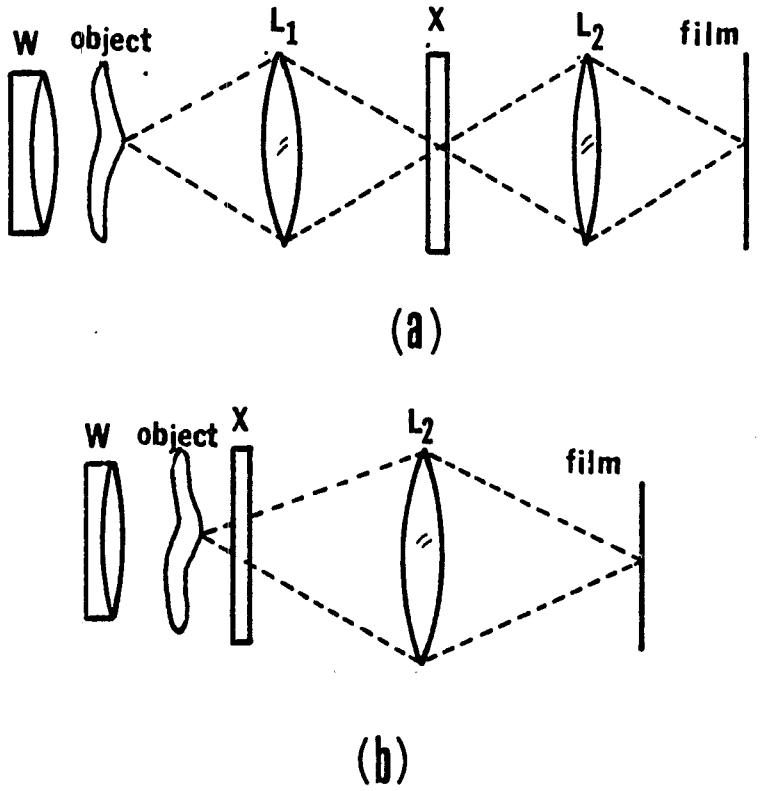

Figure 9. Schematic of two alternative setups for the second half of the NLF.

primarily affects the amplitude structure of the second SH beam. This causes the contrast to deteriorate so that the fringes are unreadable.

An experiment was performed to estimate the effect on the interferograms of (a) defocus of the image of the object on the recording plane, and (b) the shifting of the crystal with respect to the image plane as formed by lens L_1. The results are shown in Figure 10. In no case have we found fringes that were readable but had errors of more than 10%. This error is the worst we have seen, and usually there is no observable fringe distortion. Hence, we normally try the easy case of Figure 9b first, and if fringes are not observed, the setup of Figure 9a is tried next.

The $LiNbO_3$ samples used in this study do not have antireflection coatings and the high Fresnel reflection of the surfaces (about 13%) causes many spurious fringes due to multiple reflections (the refractive index of $LiNbO_3$ is about 2). To cope with these fringes, we orient the optic axis vertically in the holder in Figure 7a so we can easily rotate the crystal in the noncritical dimension. When this is done, the imaging varies across the crystal, but as noted above, this is not of great concern. We can distinguish the real NLF fringes that do not vary with rotation, from spurious ones that do vary, and we can arrange the spurious fringes so they are not bothersome. Finally, for reasons of safety, the IR beam is blocked out before the camera with a dichroic beamsplitter (not shown in the figure) that has high reflectance at $\lambda = 1.06$ μm and transmits the green light.

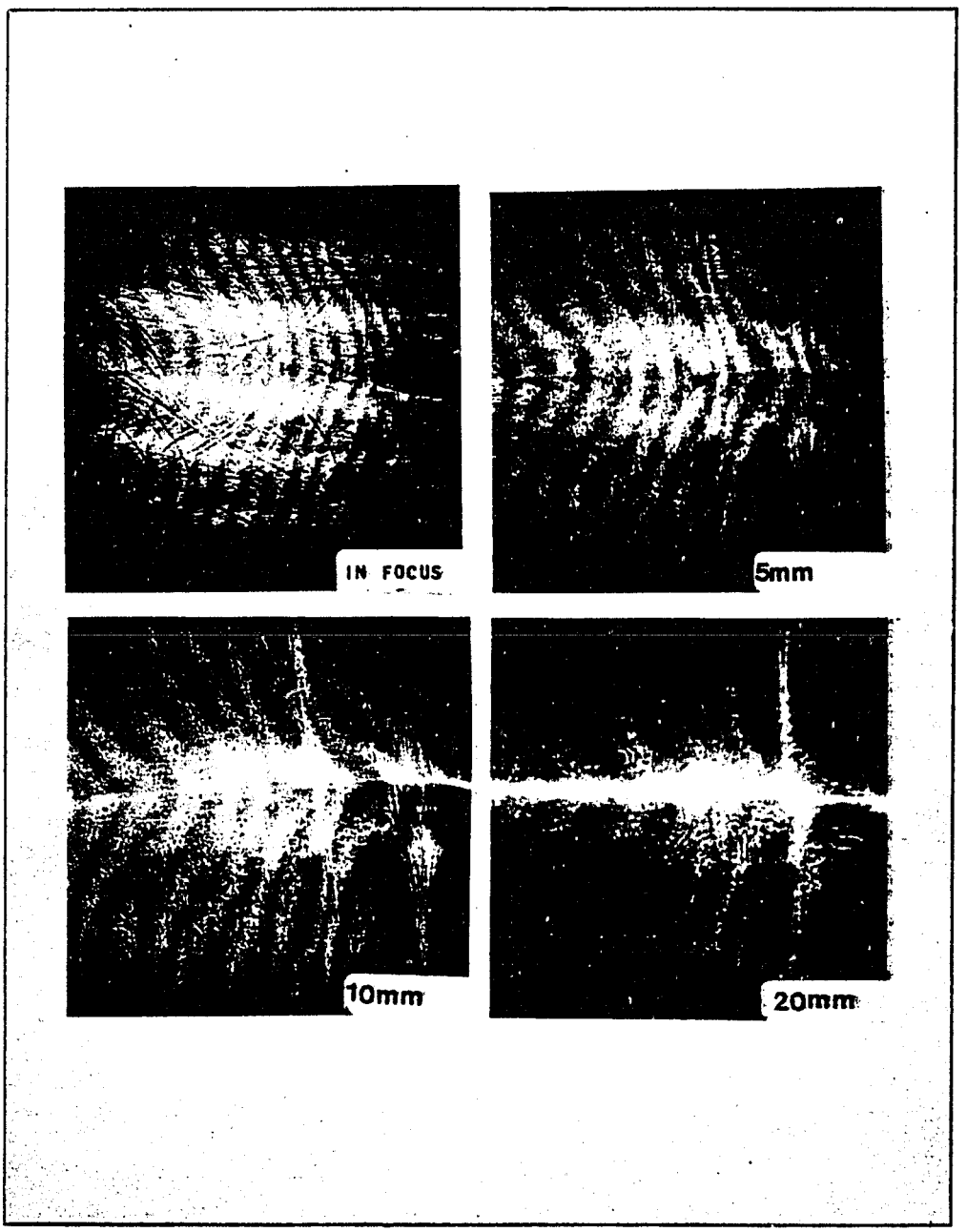

Figure 10. Effect of defocusing the object on the recording plane and the shifting of the crystal.

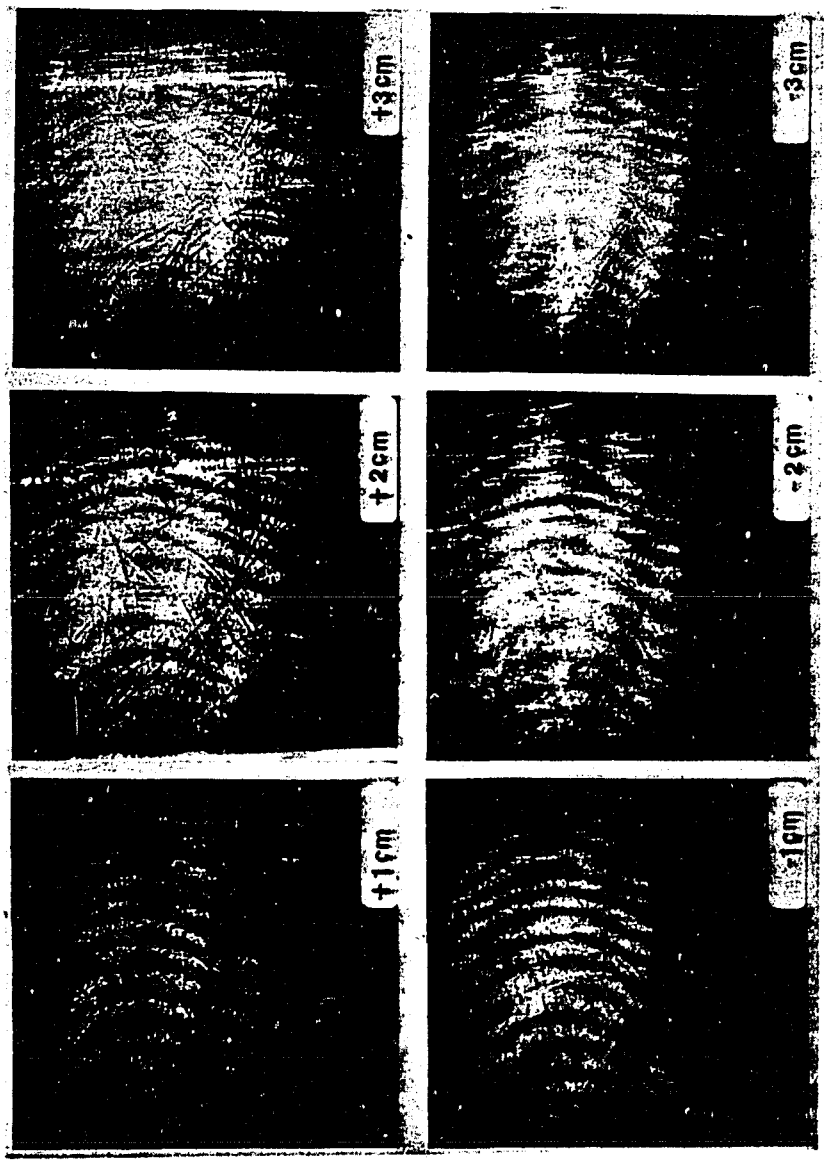

Figure 10. -- Continued

Experimental Results

Test of the Interferometer

The most straightforward application of the NLF is the measurement of the contour of lenses. We describe measurements of this kind primarily to test the NLF. In the first test, a spherical lens is contoured in a setup shown in Figure 11, which results from combining Figures 8b and 9b. After the first doubling, the two wavefronts exit from the lens with slightly different radii of curvature. When the second doubling occurs, the two SH waves interfere and produce circular fringes which are shown in Figure 12a.

The lens is made of BK-7 glass and serves as a quantitative test of the interferometer. We measured the dispersion of BK-7 by contouring a wedge of BK-7 glass in the NLF. The dispersion is given by $\Delta n = \lambda_s/\alpha_w s$ where s is the measured fringe spearation and α_w is the wedge angle. We found a value $\Delta n = 1.29 \times 10^{-2}$ which agrees with the value predicted by a Sellmeier formula (Schott Glass Data Book p. II.5). The radii of curvature of the surfaces of the simple lens were measured using a spherometer (R_1 = 60.7 cm, R_2 = 89.03 cm) and used in the lensmaker and thin lens formulae (Born and Wolf, 1975) to calculate the difference in radii of curvature of the IR and SH wavefronts. If we let ρ_m be the radius of the n'th fringe, it is straightforward to show that the area between the fringes is constant, and that

$$\rho_m^2 - \rho_{m-1}^2 = \frac{2\lambda_s}{(\frac{1}{R_1} - \frac{1}{R_2})\Delta n} \quad . \tag{26}$$

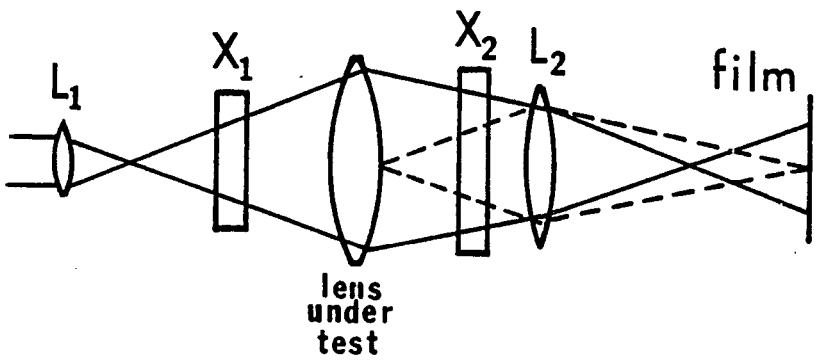

Figure 11. Schematic of the setup for testing lenses.

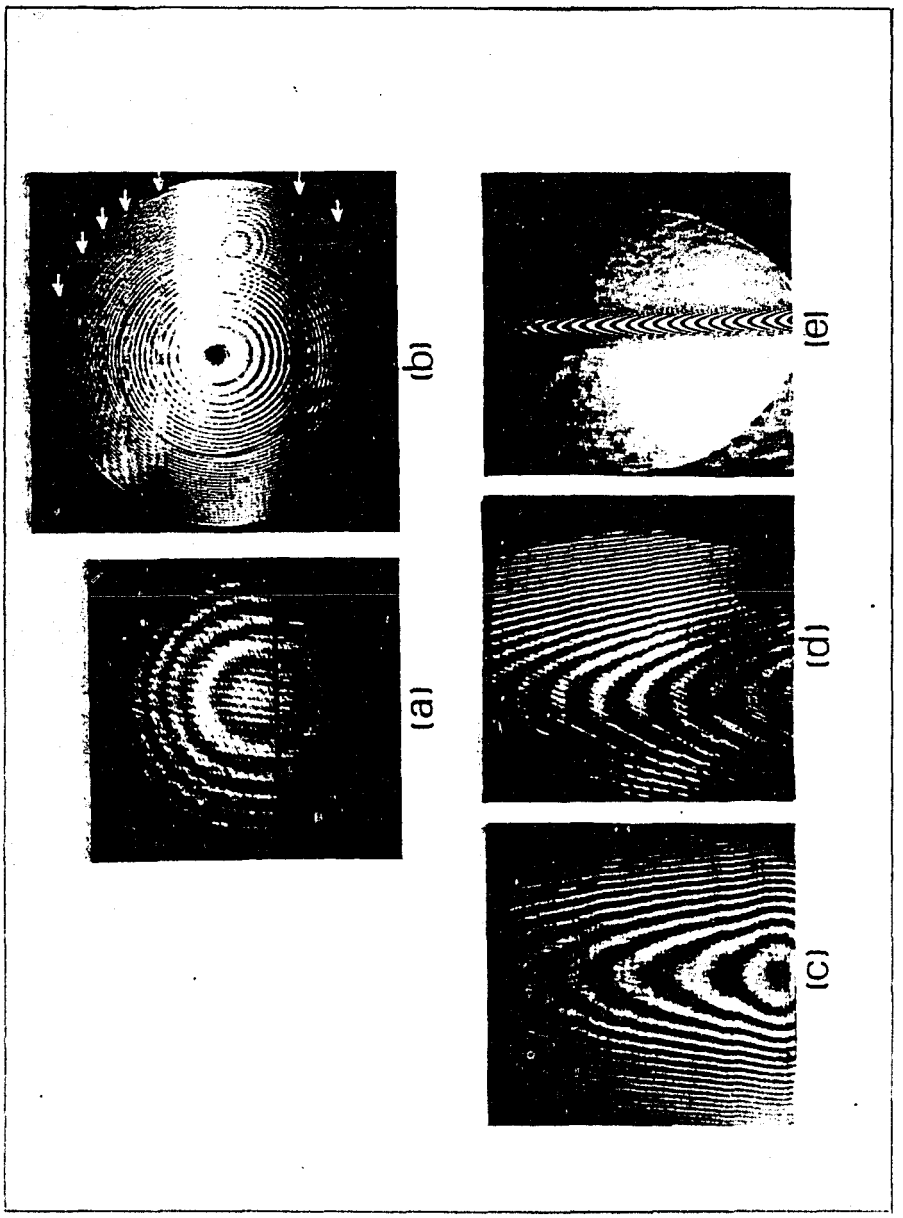

Figure 12. Interferograms produced by various lenses.

Substituting the measured values for R_1, R_2 and for Δn, we obtain $\rho_m^2 - \rho_{m-1}^2 = 29.7\ mm^2$. This value coincides with the average measured value from Figure 4a of $30.1 \pm 1.6\ mm^2$. The error is estimated by the root mean square analyses of several fringes and is due to the uncertainty ($\sim$2%) in locating the fringe.

In Figure 12b we repeat the test just described, but with a lens of f/1.0 (32 mm focal length) so that the nominal acceptance angle of the second doubler is exceeded by a factor of five. The bullseye pattern is still readable out to the edge of the lens (the lower contrast circular fringes to the right center are caused by multiple reflection from the $LiNbO_3$ and should be ignored) and hence phase matching is not, in principle, a limitation to information retrieval. There are, however, some practical points which are important, since the phase mismatch distorts the information in a systematic fashion (see Hopf et al., 1981 for theoretical details). First, note the positions labeled by the arrows in the figure. One sees that there is a horizontal line at each arrow along which the contrast vanishes. These are the locations of the Maker Fringes from the second doubler, and the amplitude of the second SH wave vanishes along these lines. The phase of the second SH wave changes by 180° at the Maker fringe so that the dark and bright fringes are interchanged. In addition, each fringe is shifted in position by a half a wave as one goes from one Maker fringe to the next. This is due to a phase shift produced by the phase mismatch in the second doubler. All of these distortions can be corrected by proper data analysis, but this is likely to be difficult

unless there is a priori knowledge of the qualitative structure of the waveform.

A cylindrical lens of 4 cm focal length was tested using a CPM $LiIO_3$ crystal for the second doubler, an NCPM crystal, and a Jamin interferometer (Murty, 1964). The setup for the NCPM test is the same as in Figure 11, except that a 2° wedge was placed before the object so that the reference fringes are horizontal. The results are shown in Figures 12c through 12e, where approximately the same area (1 x 1 cm) of the lens is shown. Note the high density of fringes in the Jamin interferometer 12e) which is the rationale for using the NLF. Notice also that in Figure 12c, where a CPM crystal was used for the second doubler, the fringes show ripples that are correlated from one fringe to the next. These ripples move with the object, and hence are not spurious noise. The ripples do not appear in Figure 12d where the NCPM crystal is used for the second doubler. Hence the ripples are not due to large defects in the lens, as would be expected from Equation 24, but reflect the differences in the way the NLF performs when CPM, rather than NCPM crystals are used for the second doubler. These ripples are caused by striae in the lens and since some ripples are barely visible in the Jamin picture, we estimate that they cause distortions in the wavefront of $\sim\lambda/20$. The local tilt of the IR wavefront in the critical dimension of the CPM crystal causes a phase mismatch between the fundamental and the SH in the second doubler. This, in turn, causes a distortion in the SH wavefront that enhances small optical perturbations as discussed in Chapter 2, so that they can be

more easily seen. This case is an example in which the asymmetry of the doubling crystal can provide a low sensitivity in one dimension and high sensitivity in another.

Transient Objects

In this test our aim is to demonstrate the capability of the NLF to study a complex transient phase object in real time. We do this by monitoring the evolution in time of the changes in dispersion that occur in a chemical reaction. The setup used for this test is shown in Figure 13, which comes from combining Figures 8a and 9b. In this setup the diaphragm d was not used in order to illustrate the consequence of leaving it out. Note the bright spot above the NLF fringes in Figure 14. This is the location of the second SH beam that does not overlap the laser beam. There is no SH produced by the second doubler in this part of the beam and hence no fringes. The wedge W has a 2° angle and produces a convenient number of straight reference fringes in the vertical direction. A cell of dimensions 30 x 17 x 3 mm is used to house the chemicals and it is placed as close as possible to the second doubler. L_2 is used to image the cell onto the film plane.

Prior to the test shown here we examined the diffusive mixing of two substances using this setup. In Figure 14a, we show an example of such a test where 0.2 ml of 58% NH_3 aqueous solution is introduced as a layer on top of 1 ml of water. The interferometer can follow the subsequent mixing without difficulty. To make the test more interesting, 0.2 ml of 99.8% pure acetic acid was added which resulted

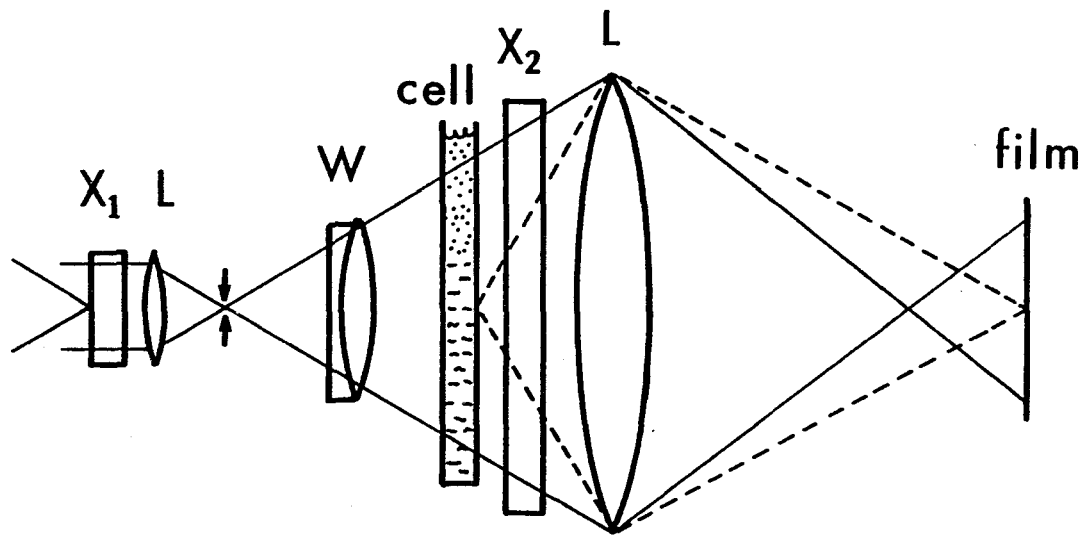

Figure 13. Experimental configuration used to monitor a chemical reaction.

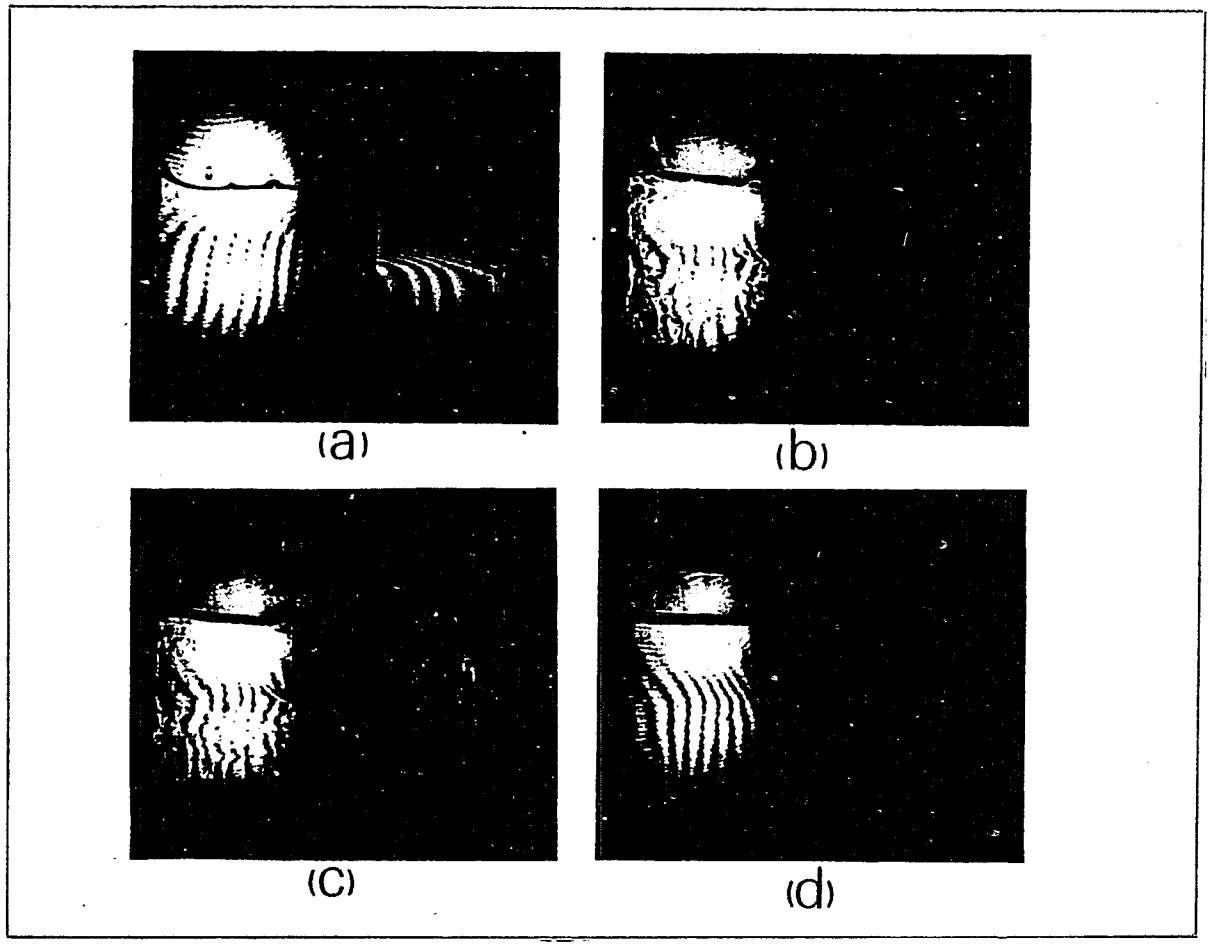

Figure 14. Comparison between the interferograms obtained with NLF and Jamin interferometers in the monitoring of an acid-base reaction.

in a vigorous acid-base reaction that brought the temperature near the boiling point. A sequence of pictures of the reaction was taken manually approximately every 2 seconds and some of these pictures are shown on the left side of Figures 14b through 14c. For comparison purposes, the test was repeated and monitored in a Jamin interferometer using the illumination of the second harmonic only and following the same procedure to take the pictures. These are on the right of each pair of pictures. The acid-base reaction induces large changes in the spatial distribution of the index of refraction made evident by the large changes in the density and shape of the fringes. The Jamin pictures become totally washed out at the most violent times in the reaction whereas the NLF pictures show fringes that can be traced at all times.

In presenting this experiment, we have qualitatively demonstrated that the NLF constitutes a potential tool in the study of rapid transient phenomena involving unusually large optical path lengths. The conventional interferometer is seen to be of little or no use in this kind of situation because the fringes are unreadable. In the experiment shown, the use of weak acids and bases means that the index changes are due primarily to the difference of indices of the reactants and components. With stronger acids and bases, more dilute solutions can be used and the contouring will be largely a measure of thermal gradients.

Refractive Objects of Peculiar Contour

In this section we show three examples of stationary refractive objects which can be usefully contoured using the NLF. The first is

a preform from which optical fibers are drawn which is a cylindrical object (8 mm dia x 25 cm long) and consists of a constant index cladding surrounding a core of graded index layers. The sample is immersed in a cell containing a liquid (n_D = 1.457) that partially matches the index of the clad and its axis is positioned transversely to the laser beam. The setup used is depicted in Figure 15 and results from combining Figures 8b and 9a. A 6.2° wedge is used that produces straight reference fringes in the horizontal direction. The sample is imaged by a spherical mirror at nearly the center of curvature and onto the second doubler X_2. The use of the mirror assures a perfect achromatism of the imaging system. Then the lens L_2 is used to relay the image of the sample to the film plane where it is recorded. The interferogram obtained is shown in Figure 16a. The many vertical lines in the center come from the layers in the core that are hard to image, but the $6.2\lambda_{S/\Delta n}$ motion in the NLF fringe is easily read. Alternate interferometric methods for preform testing either involve cutting the rod into thin slices (Martin, 1974), which is a slow process that is unreliable due to possible shattering of the preform, or shearing interferometric techniques which give slope rather than direct wavefront information (Kokubun and Iga, 1980) and operate in only one dimension. Our technique has the advantages that it is nondestructive, no axial symmetry is assumed and the fringe motion is small so that no overflowing from the interferometer field of view occurs.

In the second experiment, we contour a free-falling column of ethanol produced by a dye-laser nozzle of dimensions 1 x 0.5 mm.

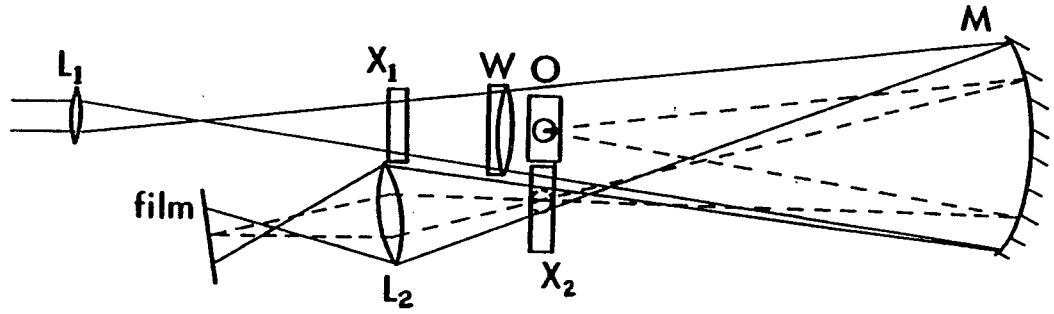

Figure 15. Schematic of the experimental setup used to contour an optical fiber preform,

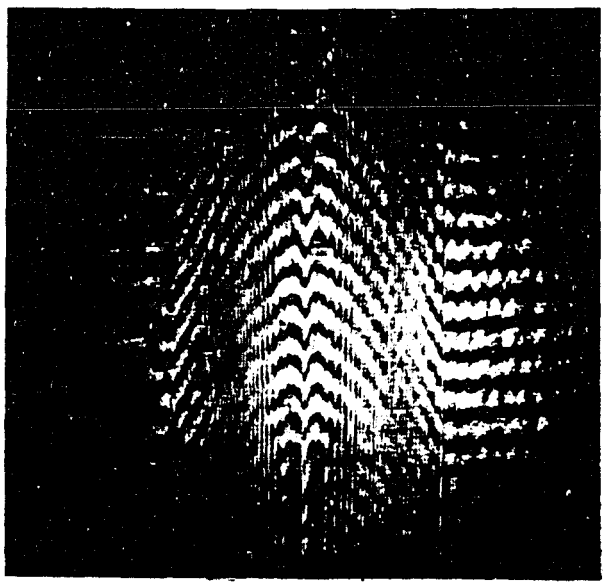

(a)

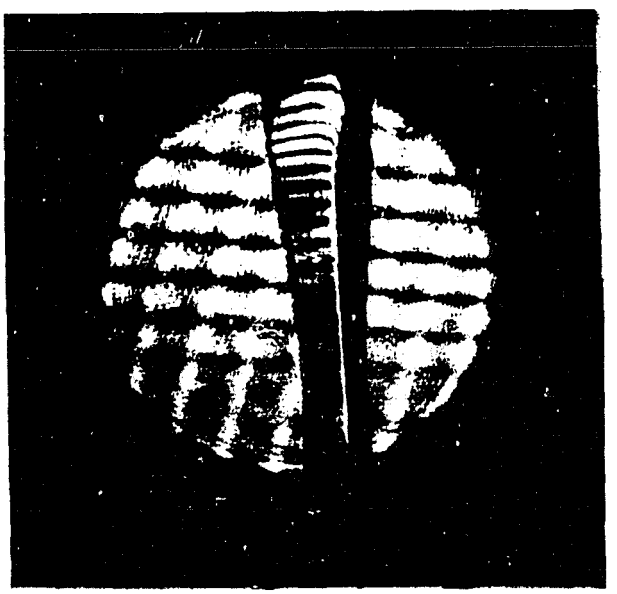

(b)

Figure 16. Interferograms of the profile of an optical fiber preform and a jet stream of alcohol.

Figure 17 shows the arrangement used for this test, which involves combining Figures 8b and 9a. In this case, the same crystal produces both SH wavefronts. The same wedge is used here as in the previous example. The jet is imaged onto the crystal by a f/0.44 spherical mirror at nearly unit magnification and then lens L_2 relays the image onto the film plane. The main difficulty we find in doing this test is that the edges of the jet are rounded, and deflect the light over a large angle. Thus a very fast mirror of short focal length ($\sim$2.5 cm) had to be used. The interferogram we obtained is shown in Figure 16b and it shows dark areas in the periphery of the jet where the light is so strongly deflected that it misses the mirror. In this and the previous example, the objects are either exactly or nearly cylindrical and when the axis of the object is oriented parallel to the optic axis of the $LiNbO_3$, the acceptance angle of the crystal is 180°.

The final test involves using the NLF in reflection as shown in the experimental setup of Figure 18. Here we contour the surface of an aluminum lap machined in a lathe and immersed in a cell containing ethanol which provides dispersion. This is basically a combination of Figures 8b and 9b except that the wedge is contained within the dispersive object (the lap is tilted at an angle θ with respect to the window of the cell) and both doublings are done with the same crystal. Here the laser beam is expanded to a diameter of about 3 cm, and the crystal is placed as close as possible to the window of the cell. The object is also as close as possible to the window. If the lap were perfectly flat, the object would act as a simple wedge with an

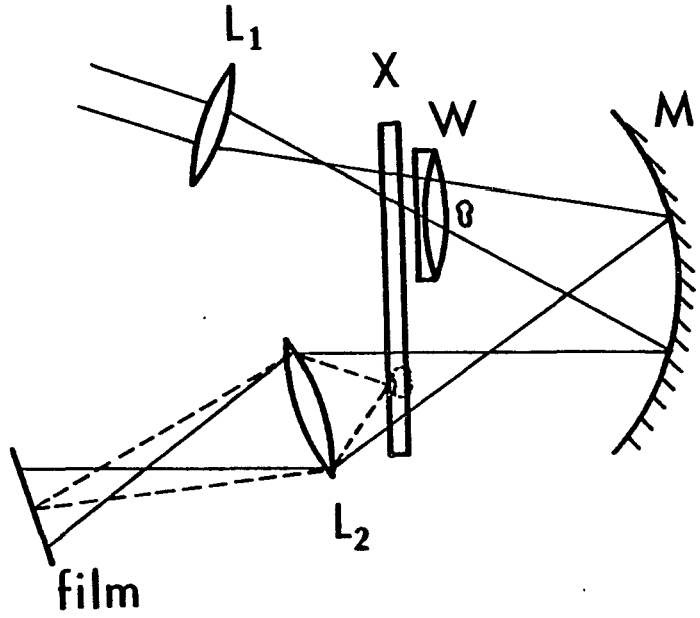

Figure 17. Schematic of the setup used to contour a jet of alcohol.

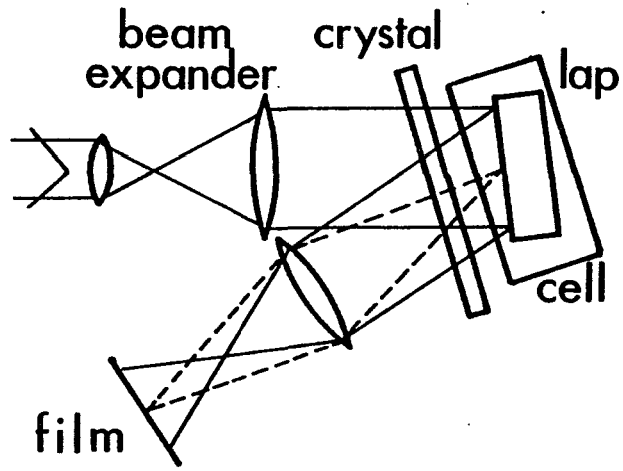

Figure 18. Schematic of the NLF in reflection.

angle 2θ, and would produce straight fringes. Any deviation from flatness of the object will cause a distortion of the fringes (i.e., a departure from straightness). In this test, a 20 μm defect was machined into the lap, and the lap was then buffed to get rid of scratches and grooves. The resulting interferogram is shown in Figure 19 along with a picture of the lap. In the interferogram, there is a fringe motion of approximately 0.7 fringe. This is consistent with the predicted value of 0.67 fringes determined by the measured (Hopf, Tomita and Al-Jumaily, 1980) dispersion of ethanol of $\Delta n = 0.88 \times 10^{-2}$.

Discussion

In this chapter we have demonstrated a breadboard version of a useful nonlinear interferometer which can be used to test dispersive phase objects with large and arbitrary changes in optical depth. The interferometer is also well suited for the study of very rapid transient events because the interferograms are obtained instantaneously and the sampling rate can be varied by changing the repetition rate of the pulsed laser. In order to record the interferograms, we used either photographic or T.V. cameras. In most cases the energy of a single pulse is sufficient to expose both satisfactorily. Being a common path interferometer, the NLF produces very stable fringes and there is no need for holographic tables.

Note that if we had used a plane wave reference (e.g., as in a Mach-Zehnder) at λ_s, the fringes would have occurred for $(n_s-1)\ell = m\lambda_s$ so that the fringes in the NLF are separated by an amount $\frac{(n_s-1)}{\Delta n}$

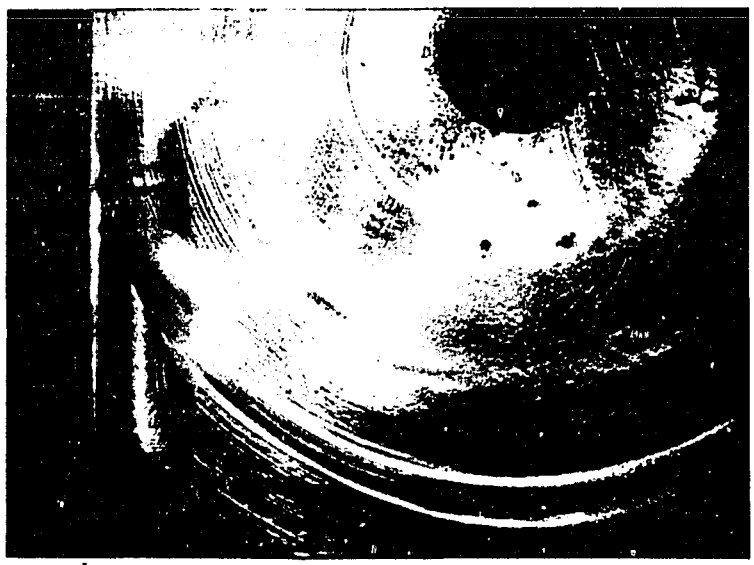

(a)

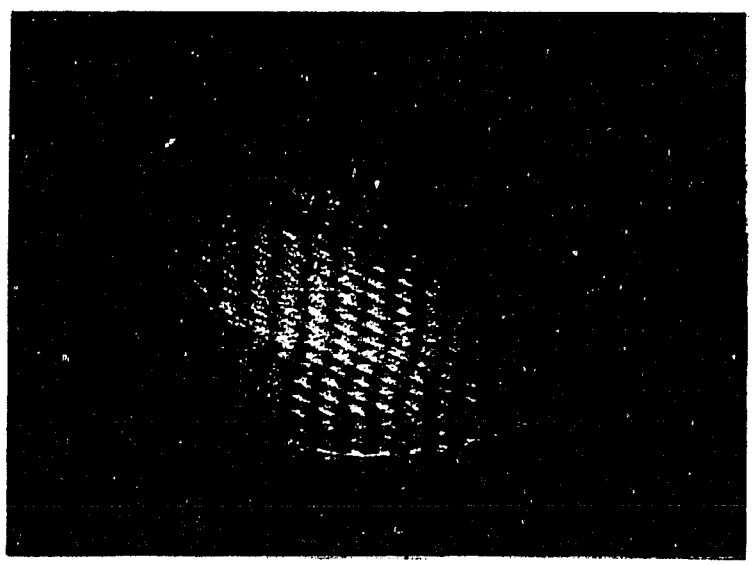

(b)

Figure 19. Picture of the metal surface and corresponding interferogram.

wider than in the Mach-Zehnder. Alternatively, we can say that the NLF is like a Mach-Zehnder with an "equivalent wavelength" $\lambda_{eq} = \lambda_S \frac{(n_s-1)}{\Delta n}$. Since Δn is ordinarily of the order of 10^{-2}, the equivalent wavelength is about $50\lambda_S$ or $\sim$ 25 μm in our case.

The interferograms obtained with the NLF are a scaled version of those obtained with a Mach-Zehnder and the same fringe pattern interpretation schemes can be applied solely by taking into account the equivalent wavelength.

One unpleasant feature of our NLF interferograms is the presence of unwanted fringes due to multiple reflections from the surfaces of the $LiNbO_3$ crystals. These can be eliminated by antireflection coats on the crystal or by spatially filtering the interferograms after the recording is made. In our experiments, we made these fringes less conspicuous by tilting the crystal in its noncritical dimension, thus making the fringes much finer than the NLF fringes.

$LiNbO_3$ is a particularly convenient material for the interferometer. Its phase-match temperature depends on its composition and we found samples that are conveniently near to room temperature. It is a nonhygroscopic material and therefore no hermetic sealing is necessary. Its transmission is high in the wavelength range of interest and it is capable of high optical quality polish.

The primary difficulty of the NLF is that the objects of interest need precise imaging due to their large spatial frequencies. Note that this is a requirement that is intrinsic to the type of object being tested, and is a limitation on all competitive schemes (IR interferometry is, however, much more forgiving with respect to

fine-scale roughness of the object). The limitations due to phase matching, which are frequently cited as a decisive obstacle to using second-order nonlinearities in birefringent crystals for optical purposes, are seen not to be a major limitation when noncritical phase matching is used. Even when the phase-match limits are exceeded, one can retrieve information about the wavefront, which is why it is difficult to assign a precise value to the acceptance angle of the nonlinear crystal. One can, however, make a few general observations about this point: for cylindrical objects, if uniaxial NCPM crystals are used, there are no angular limitations when the axis of the object is aligned parallel to the optic axis of the crystal. If one has a priori knowledge of the qualitative structure of a wavefront that varies in two-dimensions we have shown that it is possible to exceed the phase-match limitation by as much as a factor of five and extract information. For unknown wavefronts, it is safest to remain below the phase-match limitation, which in our case gives an acceptance angle of 9°.

There are a number of other aspects of the operation of the NLF that are also difficult to quantify. In principle, lasers with poor mode structure (i.e., poor spatial coherence) and crystals with very bad figure can be used, but we find that they cause so many problems in practice that we advise against using them. The laser should therefore have good mode structure, and the crystal surfaces should be reasonably flat (parallelism is not important). On the other hand, the location of the second doubling crystal at an image

plane is important in principle, but in practice this restriction can often be relaxed. This results in great simplification and flexibility of the setup.

Since the NLF contours the quantity $\Delta n\ell$, one can envision three types of applications. First, if Δn is known, one can contour ℓ. Secondly, if ℓ is known, one can determine Δn. These two types of applications have been illustrated in detail in this dissertation. A variation on this latter idea comes from noting that the laser and second harmonic polarizations are orthogonal. If the object is birefringent, then quantities like $\Delta n - (n_s^e - n_F^o)$ can be measured. These are quantities of basic interest for determining phase match angles in nonlinear optical applications. Present techniques for measuring these differences requires determining n_o and n_e separately to very high precision so that Δn may be computed to a few percent accuracy. The NLF determines these numbers directly in a single step. If Type II doublers are used for the SH steps, one can get directly the values of Δn needed to determine the Type II phase match condition. An additional application has been suggested by A. Tomita. Suppose one wants to know the contour $n_F\ell$ in the IR to considerable accuracy but finds it more convenient to measure $n_s\ell$ in the visible. One can then use an NLF interferogram whose SH wavelength is near the original visible wavelength to transfer the information to the IR with no loss in precision.

While we have shown the utility of the NLF using $LiNbO_3$ at $\lambda_F = 1.06\ \mu m$, we expect that a number of laser wavelengths and crystals capable of NCPM can be used and therefore a number of $\lambda_S/\Delta n$ values will

be available. In Table 1, the most commonly used nonlinear crystals capable of NCPM are listed along with the wavelengths at which they work, and the lasers that can be used. The $\lambda_s/\Delta n$ value for an object made of fused silica are also given.

The crystals ADP and RDA have been demonstrated experimentally to work as an NCPM material at the wavelengths shown, and both are uniaxial. These, as well as $LiSO_4 \cdot H_2O$ are commonly grown from aqueous solution, are hygroscopic and are subject to mechanical and thermal shock. Specially constructed ovens are usually required that house the crystal in a sealed cell. Since these crystals are normally used for high efficiency doubling, typical housings appear as in Figure 2b which have small, clear apertures and large lengths. These cause serious problems in vignetting when used in the NLF, and restrict the optical and physical access to the crystal which limits the flexibility of the interferometer. For NLF applications, different kinds of sealed cells are needed.

$LiSO_4 \cdot H_2O$ is biaxial, and its application is based on calculation rather than direct demonstration. The use of biaxial crystals has not been discussed in this article. They can be used in the NLF, but the restrictions on the acceptance angle are somewhat more severe because both directions of tilt are critical. The lack of a non-critical dimension prohibits the tilting of the crystal to an angle sufficiently large to make the spurious fringes less annoying. Hence, AR coats must be used. In addition to the crystals in Table 1, there are a very large number of NCPM cyrstals which can be used in conjunction with

Table 1. Laser wavelength, NCPM crystal and the $\lambda_S/\Delta n$ values for an object of fused silica, for various fixed wavelength lasers

λ_F(nm)	Crystal	Laser	$\lambda_S/\Delta n$ for fused silica, μm's
530	ADP[a,b]	Nd:Yag (doubled)	10
690	RDA[c]	Ruby	23
1064	$LiNbO_3$	Nd:Yag	73
1300	$LiSO_4 \cdot H_2O$[d]	Nd:Yag, I_2	93.6

[a] J. M. Yarborough and E. O. Ammann (IEEE J. Quantum Electron, J-QE9) 661 (1973)

[b] V. D. Volosov, V. N. Krylov, V. A. Serebryakov, and D. V. Sokolov, JEPT Lett. 19, 23 (1974)

[c] K. Kato, IEEE J. Quantum Electron, QE-10, 622 (1974)

[d] G. Al-Jumaily, personal communication, Grad Student, Optical Sciences, (1981)

pulsed dye lasers, such as the biaxial $KNbO_3$ (Günter, 1979) with a $\lambda_s/\Delta n$ value of 37 μm which works in the 850-950 nm range. Note that while none of the crystals in Table 1 are as good as $LiNbO_3$, they are the best that are available at the present time at these wavelengths.

CHAPTER 4

CONCLUSION

The NLF interferometer has been used to test a number of objects that cannot be contoured in a practical way by conventional interferometers. The low density of fringes, ease of alignment, real-time capability, as well as the fact that it is self-referencing make this instrument a potentially useful tool in the study of a wide variety of objects of which we have selected a few as representative. We have shown that there is no need for exceptionally high quality crystals to apply this technique and that crystals of acoustic grade $LiNbO_3$ performed well.

We have also tested the concept of two Second harmonic interferometers in which phase mismatching of the doubling process is used to measure local wavefront tilts. These are suited for testing the degree of colimation of a wavefront with small curvature. The Nonlinear induced shear interferometer is able to detect a wavefront distortion of the order of 1/20 of visible wavelength. The Maker fringe interferometer is easy to operate and is particularly useful for detecting small changes in the wavefront curvature of unexpanded Gaussian beams and for locating the beam waist accurately, tasks that shearing interferometers do not perform as well.

REFERENCES

Armstrong, J. A., N. Bloembergen, J. Ducuing and P. S. Pershan. "Interactions between Light Waves in a Nonlinear Dielectric", Phys.Rev. 127; 1918 (1962).

Ashkin, A., G. D. Boyd, J. M. Dziedzic, R. G. Smith, A. A. Ballman, J. J. Levinstein, and K. Nassau. "Optically-induced Refractive Index Inhomogeneities in $LiNbO_3$ and $LiTaO_3$", Appl. Phys. Lett. 9, 72 (1966).

Bar-Joseph, I., A. Hardy, Y. Katzir, and Y. Silberberg. "Low-Power Phase-Conjugate Interferometry", Opt. Lett. 6, 414 (1981).

Bloembergen, N., and P. S. Pershan. "Light Waves at the Boundary of Nonlinear Media". Phys. Rev. 128, 606 (1962).

Boyd, G. D., R. C. Miller, K. Nassau, W. L. Bond, and A. Savage. "$LiNbO_3$: an Efficient Phase Matchable Nonlinear Optical Material". Appl. Phys. Lett., 5, 234 (1964).

Chang, R. K., J. Ducuing, and N. Bloembergen. "Relative Phase Measurement between Fundamental and Second-Harmonic Light" Phys. Rev. Lett. 15, 6 (1965).

Franken, P. A., A. E. Hill, C. W. Peters, and G. Weinreich. "Generation of Optical Harmonics." Phys. Rev. Lett. 7, 118 (1961).

Giordmaine, J. A. "Mixing Light Beams in Crystals". Phys. Rev. Lett. 8, 19 (1962).

Geusic, J. E., H. M. Marcos, and L. G. Van Uitert, "Laser Oscillations in Nd:doped yttrium aluminum, yttrium galium, and gadolinium garnets". Appl. Phys. Letts. 4, 182 (1964).

Günter, P. "Near-Infrared noncritically phase-matched second-Harmonic generation in $KNbO_3$", Appl. Phys. Lett., 34, 650 (1979).

Hellwarth, R. W., "Generation of Time Reversal Wavefronts by Nonlinear Refraction". J. Opt. Soc. Am., 67, 1 (1973).

Hopf, F. A., A. Tomita, and G. Al-Jumaily, "Second Harmonic Interferometers" Optics Lett. 5, 386 (1980).

Hopf, F. A., "Interferometery using Conjugate-Wave Generation" J. Opt. Soc. Am., 70, 1320 (1980).

Hopf, F. A., A. Tomita, G. Al-Jumaily, M. Cervantes, and T. Liepmann, "Second Harmonic Interferometers II", Opt. Commun. 36, 487 (1981).

Hopf, F. A., and M. Cervantes. "A Useful Nonlinear Optical Interferometer" Appl. Opt. (in press).

Kim, B., and C. S. Tsai. "High Performance Guided-Wave Acousto-optic Scanning Devices using Multiple Surface Acoustic Waves". Proc. IEEE 64, 788 (1976).

Kokubun, Y., and K. Iga "Refractive-Index Profile Measurement of Preform Rods by a Transverse Differential Interferogram" Appl. Opt. 19, 846 (1980).

Kushida, T. , H. M. Marcos, and J. E. Geusic, "Laser Transition Cross-section and Fluorescence Branching Ratio for Nd^{3+} in Yttrium Aluminum Garnet". Phys. Rev. 167, 1289 (1968).

Lam, S. S., C. Koliopoulos, and J. C. Wyant. Optical Metrology with Two-Wavelength Real-Time Holography, Abst. J of Opt Soc Am, Dec 1980.

Lean, E. G. H., J. M. White, C. D. Wilkinson. "Thin-film Acousto-optic Devices" Proc. IEEE 64, 779 (1976).

Maker, P. D., R. W. Terhune, M. Nissenof, and C. M. Savage, "Effect of Dispersion and Focusing on the Production of Optical Harmonics" Phys. Rev. Lett. 8, 21 (1962).

Martin, W. E. "Refractive Index Profile Measurements of Diffused Optical Waveguides." Appl. Opt. 13, 2112 (1974).

Miller, R. C., G. D. Boyd, and A. Savage. "Nonlinear Optical Interactions in $LiNbO_3$ without Double Refraction", Appl. Phys. Lett. 6, 77 (1965).

Miller, R. C., and W. A. Nordland. "Absolute Signs of Second-Harmonic Generation Coefficients of Piezoelectric Crystals", Phys. Rev. B2, 4896 (1970).

Miller, R. C., and W. A. Nordland. "Further Measurements of Absolute Signs of Second-Harmonic-Generation in Piezoelectric Crystals". Phys. Rev. B5, 4931 (1972)

Munnerlyn, C. R., and M. Latta. "Rough Surface Interferometry Using a CO_2 Laser Source". Appl. Opt. 7. 1858 (1968).

Murty, M.V.R.K. "Some Modifications of the Jamin Interferometer Useful in Optical Testing". Appl. Opt. 3, 535 (1964).

Nath, G., and S. Maussühl "Large Nonlinear Optical Coefficient and Phase Matched Second Harmonic Generation in $LiIO_3$". Appl. Phys. Lett. 14, 154 (1969).

Rossi, B. Optics, Addison and Wessley, Reading, 1962, p. 296.

Schott Glass Databook, p. II-5. Schott Optical Glass, Inc., Fullerton, CA (1979).

Singh, S., W. A. Bonner, J. R. Potopowicz, and L. G. van Uitert, "Nonlinear Optical Susceptibility of Lithium Formate Monohydrate", Appl. Phys. Lett. 17, 292 (1970).

Tsuruta, T. S., N. Shiotake, J. Tsujiuchi, and K. Matsuda. "Holographic Generation of Contour Map of Diffusely Reflecting surface by Using Immersion Technique", Jap. J. Appl. Phys. 6, 661 (1967).

Wyant, J. C. Holographic and Moire Techniques in Optical Shop Testing. D. Malacara Ed. (Wiley, New York 1978) p. 381.

Wynne, J. J., and N. Bloembergen. "Measurement of the Lowest-Order Nonlinear Susceptibility in III-V Semiconductors by Second-Harmonic Generation with a CO_2 Laser". Phys. Rev. 188, 1211 (1969).

Yariv, A. "Transmission and Recovery of Three-Dimensional Image Information in Optical Waveguides," J. Opt Soc. Am. 66, 301 (1976).

Zernike, F. "Refractive Indices of Ammonium Dihydrogen Phosphate and Potassium Dihydrogen Phosphate between 2000 Å and 1.5 μm. J. Opt. Soc. Am. 54, 1215 (1964).

Zernike, F., and J. E. Midwinter. Applied Nonlinear Optics (Wiley, New York, 1978).